ISSN 0016-7029, Geochemistry International, 2017, Vol. 55, No. 8, pp. 683–710. © Pleiades Publishing, Ltd., 2017.
Original Russian Text © M.V. Luchitskaya, B.V. Belyatsky, E.A. Belousova, L.M. Natapov, 2017, published in Geokhimiya, 2017, No. 8, pp. 685–714.

Composition and Geodynamic Setting of Late Paleozoic Magmatism of Chukotka

M. V. Luchitskaya[a], *, B. V. Belyatsky[b], **, E. A. Belousova[c], *, and L. M. Natapov[c], ******

[a] Geological Institute (GIN), Russian Academy of Sciences, Pyzhevskii per. 7, Moscow, 119017 Russia
[b] Center for Isotopic Research, Karpinskii All-Russia Research Institute of Geology, Srednii pr. 74, St. Petersburg, 199106 Russia
[c] GEMOC ARC National Key Centre, Department of Earth and Planetary Sciences, Macquarie University, NSW 2109, Sydney, Australia

*e-mail: luchitskaya@ginras.ru
**e-mail: bbelyatsky@mail.ru
***e-mail: elena.belousova@mq.edu.au
****e-mail: lev.natapov@mq.edu.au

Received October 24, 2016; in final form, December 14, 2016

Abstract—The paper reports the results of petrogeochemical and isotope (Sr-Nd-Pb-Hf) study of the Late Paleozoic granitoids of the Anyui–Chukotka fold system by the example of the Kibera and Kuekvun massifs. The age of the granitoids from these massifs and granite pebble from conglomerates at the base of the overlying Lower Carboniferous rocks is within 351–363 Ma (U-Pb, TIMS, SIMS, LA-MC-ICP-MS, zircon) (Katkov et al., 2013; Luchitskaya et al., 2015; Lane et al., 2015) and corresponds to the time of tectonic events of the Ellesmere orogeny in the Arctic region. It is shown that the granitoids of both the massifs and granite pebble are ascribed to the I-type granite, including their highly differentiated varieties. Sr-Nd-Pb-Hf isotope compositions of the granitoids indicate a contribution of both mantle and crustal sources in the formation of their parental melts. The granitic rocks of the Kibera and Kuekvun massifs were likely formed in an Andean-type continental margin setting, which is consistent with the inferred presence of the Late Devonian–Early Carboniferous marginal-continental magmatic arc on the southern Arctida margin (Natal'in et al., 1999). Isotope data on these rocks also support the idea that the granitoid magmatism was formed in a continental margin setting, when melts derived by a suprasubduction wedge melting interacted with continental crust.

Keywords: granitoids of the Kibera and Kuekvun massifs, I-type granites, Anyui–Chukotka fold system, Chukotka–Arctic Alaska microcontinent, Sr–Nd–Pb isotope systematics, Hf isotope composition of zircon

DOI: 10.1134/S0016702917080043

INTRODUCTION

The studied objects are located in the Anyui–Chukotka fold system, which is one of the main tectonic elements of the Mesozoides of Northeast Asia. It is hidden beneath the East Siberian and Chukchi seas in the north, bounded by the South Anyui fold system in the southwest, and overlain by the Upper Cretaceous volcanics of the Okhotsk–Chukotsk volcanic belt in the south and southeast (Fig. 1). The Anyui–Chukotka fold system is a fragment of the passive margin of the Chukotka (Chukotka–Arctic Alaska) microcontinent and consists of the Paleozoic–Mesozoic platform and shelf rocks. Paleozoic rocks comprise Middle Ordovician–Middle Carboniferous carbonate, carbonate–terrigenous, and terrigenous sediments, which were metamorphosed under the amphibolite and green-schist facies conditions in uplifts (granite–metamorphic domes) (Gel'man, 1995). In the eastern part of the Anyui–Chukotka fold system (Koolen dome, East Chukotka), highly deformed Precambrian rocks underwent to the green-schist and amphibolite facies metamorphism are exposed at the base of the sequence (*Geodynamics* ..., 2006). Thick Triassic flyschoid terrigenous sequences are predominant in the Anyui–Chukotka fold system. Separate basins are filled with the Upper Jurassic–Lower Cretaceous volcanogenic–terrigenous rocks. In the Early Cretaceous, the passive margin of the Chukotka microcontinent collided with an active margin of the North Asian (Siberian) continent along the South Anyui suture, which marks the closure of residual oceanic turbidite basin (Sokolov et al., 2015).

Late Mesoizoic granitoid complexes occupy 10% of the Anyu–Chukotka fold system. Granitoid plutons intrude Devonian–Carboniferous and Late Permian–Triassic folded sedimentary complexes, as well as variably deformed sediments of Late Jurassic–Early Cretaceous basins. In the geological maps, all granitoid complexes of the Chukotka Mesozoides are ascribed to the Upper Cretaceous Chukchi (West Chukotka) or Taureran (East Chukotka) complexes (*State ...,* 1984; Tibilov and Cherepanova, 2001; Varlamova et al., 2004].

New geochronological data confirm the earlier stated concepts of the presence of Paleozoic granitoids in Chukotka (Ditmar, 1938; Tibilov et al., 1986; Natal'in et al., 1999) and indicate the wider scales of Late Paleozoic granitoid magmatism (Polzunenkov et al., 2011; Akinin et al., 2011; Katkov et al., 2013; Luchitskaya et al., 2015; Lane et al., 2015). This reflects the need to characterize the compositional features of the Late Paleozoic granitoids and their magma sources, and to determine their geodynamic setting. These data will help us to trace the evolution of the granitoid magmatism of the region from Late Paleozoic to the Late Mesozoic.

This paper reports the results of petrogeochemical and isotope (Sr–Nd–Pb–Hf) study of the Late Paleozoic granitoids of the Anyui–Chukotka fold system by the example of the Kibera and Kuekvun massifs, whose age was reliably substantiated by U–Pb SIMS and TIMS zircon dating (Luchitskaya et al., 2015). Petro and isotope-geochemical characteristics of the granitoids were used to reconstruct the geodynamic setting of their formation.

BRIEF GEOLOGICAL DESCRIPTION

The studied Paleozoic granitoids are confined to the central parts of the Kuul and Kuekvun uplifts of the Anyui–Chukotka fold system, where complexes of crystalline basement and Paleozoic cover of the Chukotka microcontinent are exposed.

The Kuul Uplift is located in the northern part of the Anyui–Chukotka fold system and extended in the WNW direction for 110 km along the coast at a width up to 15–30 km (Fig. 1a). The central part of the uplift exposes mainly Devonian terrigenous and Lower–Middle Carboniferous terrigenous–carbonate sequences, which with stratigraphic unconformities are overlain by the Upper Permian–Triassic terrigenous rocks.

The Lower–Middle Devonian terrigenous rocks and Upper Devonian carbonate–terrigenous rocks are observed in the western part of the Kuul Uplift, in the coastal cliffs of the Cape Kibera area (Fig. 1b) (coast of the East Siberian Sea). The Lower–Middle Carboniferous terrigenous–carbonate complexes lay on the Upper Devonian rocks with stratigraphic unconformity and erosion: the base consists of 7-m thick conglomerates with pebble and boulders of gangue quartz, quartzite, shales, sandstones, limestones, and granites (*State,* .... 1984; Tibilov et al., 1986, *Geodynamics* ..., 2006). The youngest stratified rocks of the Cape Kibera area are Permian–Triassic sandy-clayey sediments, which with a hiatus but without visible angular unconformity rest on the Lower–Middle Carboniferous rocks.

The Devonian rocks are intruded by the Kibera granitoid massif (Fig. 1b); the massif is 15 km^2 in exposed area; its larger portion is possibly buried beneath the shelf rocks of the East Siberian Sea (Tibilov and Cherepanova, 2001).

The Kibera Massif is made up mainly of biotite granite and granodiorite related by gradual transitions; and less common subalkaline granite. The granite and granodiorite contain more melanocratic rounded enclaves from 10 to 50 cm across, which have the finer grained texture as compared to host granites and chemically correspond to monzonite. A zone of contact-metamorphic rocks around few hundred meters thick is observed in the northwestern contact of the massif with the Upper Devonian clastic rocks. According to our observations, the inner near-contact part of the massif around 500 m thick was presumably partially tectonized and consists of medium-grained gneissic granodiorite. Tibilov et al. (1986) supposed zoned structure of the massif and distinguished the inner contact zone up to 1.5 km wide.

The Kuekvun Uplift is extended in the sublatitudinal direction for 90 km at a width of 25 km (Figs. 1a, 1c). Metamorphosed Devonian–Middle Carboniferous terrigenous rocks exposed in the central part of the uplift are conformably overlain by the Upper Permian–Lower Triassic sequences (Varlamova et al., 2004). According to P.L. Tikhomirov (Kulyukina et al., 2013), the contact between metamorphic and non-metamorphic rocks are tectonic. According to (Kulyukina et al., 2013), the Devonian–Middle Carboniferous rocks were metamorphosed at 560–600°C and 2.5–4 kbar.

In the southeastern part of the uplift, the metamorphic rocks according to (Varlamov et al., 2004) were intruded by granitoids forming a massif 30 × 10 km in size, which we termed the Kuekvun Massif. In its

Fig. 1. Geological scheme of Central Chukotka modified after (Tibilov and Cherepanova, 2001) (a) and geological maps of the Cape Kibera (b) and Kuvet–Kuekvun interfluve areas (c), compiled using materials (Varlamova et al., 2004; *State...,* 1984). (a): (*1*) Anyui–Chukotka fold system: (*2*) South Anyui suture zone; (*3*) Alazei–Oloi fold system; (*4*) Okhotsk–Chukotka volcanic belt; (*5, 6*) granitoids: (*5*) – Cretaceous; (*6*) Late Paleozoic; (*7*) faults. Letters denote uplifts: (A) Alyarmaut, (KU) Kuul, (K) Kuekvun. (b, c): (*1*) Quaternary rocks; (*2, 3*) Devonian terrigenous rocks: (*2*) Lower–Middle Devonian, (*3*) upper Devonian; (*4*) Devonian–Carboniferous sedimentary and metamorphic complexes; (*5*) Lower–Middle Carboniferous terrigenous–carbonate rocks; (*6*) Upper Permian–Triassic terrigenous rocks; (*7*) Lower Cretaceous volcanogenic–sedimentary rocks; (*8*) Late Paleozoic granitoids of the Kibera and Kuekvun massifs; (*9*) dikes and bodies: (*a, b*) Early Triassic gabbrodiabase and gabbro, (*c*) Late Cretaceous diorite; (*10*) faults: (*a*) thrust faults, (*b*) others; (*11*) dip and strike.


(a)
EAST SIBERIAN SEA
165°
168°
171°
174°
70°
180°
69°
68°
Cape Kibera
Chauna bay
KU
K
A
100 km
1
2
3
4
5
6
7
(b)
N
Shelaurova I.
Cape Kibera
0 1 km
(c)
Mt. Bol'shaya
10 km
8
9
10
11

northern framing, we studied low-angle thin (up to few tens of meters) bodies of light-gray granitoids, which were transformed into augen gneiss or granite gneiss with "orbicules" of K-feldspar, plagioclase, and quartz.

The geochronological studies of the granitoids of the Kibera and Kuekvun massifs, as well as granite pebble from conglomerates at the base of Carboniferous rocks defined Early Carboniferous (352–359 Ma) (U-Pb, TIMS, and SIMS, zircon, Katkov et al., 2013; Luchitskaya et al., 2015) or Late Devonian–Early Carboniferous ages (351–363 Ma), (U-Pb, TIMS, and LA-MC-ICP-MS, zircon, Lane et al., 2015). The obtained age dates agree with the time of the Ellesmere Orogeny in the Arctic region.

ANALYTICAL METHODS

The major-element composition of the granitoids was analyzed at the chemical analytical laboratory of the Geological Institute of the Russian Academy of Sciences using XRF method on a successive Bruker S4 Pioneer sequential spectrometer and Spectra-Plus software. The contents of major oxides were analyzed in the following intervals (in wt %): SiO_2 1.0–99.5, TiO_2 0.01–5.0, Al_2O_3 1.0–60.0, Fe_2O_3 1.0–40.0, MnO 0.01–1.0, CaO 1.0–50.0, MgO 0.1–40, Na_2O 0.1–10.0, K_2O 0.1–10.0, and P_2O_5 0.01–5.0. A method of fundamental parameters was used to take into account matrix effects in the Spectra-Plus software. Standard samples (GSO, OSO, MSO) close in composition to the analyzed samples (felsic, intermediate, and mafic) were used as comparison samples. The calibration plots were constructed using 50 standard samples of different composition. The procedure of sample preparation for analysis and statistic parameters of accuracy and correctness correspond to the recommendations of certified technique NSAM No. 439-RS MPR RF.

Trace element composition of the granitoids was determined at the Analytical Center of the Institute of the Technology of Microelectronics and Ultrapure Materials of the Russian Academy of Sciences. Mafic rocks were decomposed in an open system, while samples of felsic composition were analyzed in an autoclave MKP-05 NPVF (ANKON-AT-2, Russia). To control the complete dissolution of samples and possible losses during decomposition, each analyzed sample was doped with stable highly enriched ^{161}Dy and ^{62}Ni. The contents of trace elements in obtained solutions were determined by inductively coupled plasma atomic emission spectrometry (ICAP-61, *Thermo Jarrell Ash*, US), and inductively coupled plasma mass spectrometry (X-7, *Thermo Elemental*, US). Relative standard deviation for all analyzed elements was no more than 0.2 for element contents below the five-fold detection limit and below 0.1 for contents above the five-fold detection limit. The correctness of the analyses was verified by the measurement of standard samples: essexite gabbro SGD-1A (GSO 521-84P); essexite gabbro SGD-2A (GSO 8670-2005); albitized granite SG-1a (GSO520-84P); and alkaline agpaitic granite SG-3 (GSO3333-85).

Sr, Nd, and Pb isotope compositions were determined at the Center for Isotopic Research, Karpinskii All-Russia Research Institute of Geology (St. Petersburg). The contents of Rb, Sr, Sm, and Nd were analyzed in 50–100-mg aliquots of granitoid samples. The aliquots were mixed with isotope tracer ^{149}Sm-^{150}Nd + ^{87}Rb-^{84}Sr and dissolved in a mixture of HF + HNO_3 + $HClO_4$ at 120°C in autoclave during five days. Further separation of the elements for mass spectrometric analysis was performed using ion-exchange and chromatographic separation of elements (Richard et al., 1976). The total blank during measurement was 0.01 ng for Rb, 0.2 ng for Sr, 0.01 ng for Sm, and 0.05 ng for Nd, which did not affect significantly the isotope ratios of measured elements.

The Rb, Sr, Sm, and Nd isotope ratios were measured on a TRITON thermoionization mass spectrometer (Thermo) using a double filament in a static multicolector mode at an accelerating voltage of 10 kV. 50-mg NIST 987 or 100 ng JNdi-1 international standards were measured prior to each run. The average accuracy of the analyses was 0.002% (2 σ) for ^{87}Sr/^{86}Sr isotope ratio and 0.005% (2 σ) for ^{143}Nd/^{144}Nd ratio. Concentrations measured by isotope dilution and ^{87}Rb/^{86}Sr and ^{147}Sm/^{144}Nd ratios were calculated using Excel2003. Measurement error was 1%.

For study of Pb isotope composition, the whole-rock granitoid samples were decomposed in a mixture of concentrated HF + HNO_3 (5 : 1) in a closed Teflon beaker in oven for 24 hr at 150°C (sample weight of 150–350 mg), then were dissolved in HCl in an open Teflon beaker on an electric furnace at temperature of 80–90°C in a laminar flow bench. Lead was extracted on a micro-columns filled with 100 μL Eichrom Sr Spec ion-exchange resin (Germany) in HCl. Extracted fractions of lead in HNO3 form were loaded onto a Re filament in a mixture of silicagel and 1 μL 0.2N H_3PO_4.

The Pb isotope composition was measured on a solid-phase Thermo TRITON mass-spectrometer in a single filament multichannel mode. The ion currents of 204, 206, 207, and 208 Pb isotopes were measured. Each measurement included 50 blocks of 10 scans at a Re filament current of 2.2–2.3 A at 1300°C. The 100-ng NIST 981 standard (standard aliquot corresponds to the average content of released Pb of a sample) was analyzed prior to and after each measurement session. The average accuracy of the analyses corresponded to 0.05% (2σ) for ^{206}Pb/^{204}Pb ratio. The isotope ratios were corrected for current apparatus mass fractionation using the average values of the NIST 981 measurements (^{206}Pb/^{204}Pb = 16.9374,

$^{207}Pb/^{204}Pb$ = 15.4916, $^{208}Pb/^{204}Pb$ = 36.7219) obtained at temperature of sample analysis on a filament source. The measured Pb isotope ratios were corrected for standard mass-fractionation for given device (estimate of long-term mass-fractionation at complete evaporation of standard aliquot): 0.120% per 1 a.m.u. for $^{206}Pb/^{204}Pb$ and $^{207}Pb/^{204}Pb$; and 0.135% per 1 a. m. u. for $^{208}Pb/^{204}Pb$. The average blank during the measurements was no more than 0.02 ng for Pb, while its isotope composition was $^{206}Pb/^{204}Pb$ = 18.120, $^{207}Pb/^{204}Pb$ = 15.542, $^{208}Pb/^{204}Pb$ = 37.354. The blank to sample lead ratio usually was no more than 1/200000. In this case, the correction for the content of blank Pb for measured lead isotope ratios was not incorporated; at lower Pb contents in samples, the correction for blank was performed in an "off-line regime" of calculation of measured Pb isotope ratios.

The Lu–Hf isotope composition of the zircons was analyzed in situ at the GEMOC center of the Macquarie University (Sydney, Australia) by UV New Wave UP 213nm laser coupled with a Nu Plasma ICP MS multi-collector mass spectrometer. The diameter of the ablation crater was ~50 μm. All analytical measurements were made in helium. Initial $^{176}Lu/^{177}Hf$ ratios were calculated from measured $^{176}Lu/^{177}Hf$. The error (2σ) of single $^{176}Lu/^{177}Hf$ analysis was ~±1–2%, including the error of analytical uncertainties and spatial variations of the Lu/Hf distribution in zircons. The description of technique details, methodical approaches, and constants used for the performance of εHf calculations and model ages $\left(T^{C}_{\mathrm{DM}}\right)$, as well as the reference to original works are given in (Kuznetsov et al., 2009).

PETROGEOCHEMISTRY OF GRANITOIDS

Major and trace element data on the granitoids of the Kibera and Kuekvun massifs, as well as granite pebble from conglomerate at the base of the Carboniferous sequence are shown in Table 1. The SiO_2 contents in the granitoids from the Kibera and Kuekvun massifs and from pebble are, respectively, 67–76, 56–76, and 64–73 wt %. In terms of $K_2O–SiO_2$ relations, the granitoids of the Kibera Massif and from pebble are ascribed to the calc-alkaline and high-K calc-alkaline series, while those of the Kuekvun Massif belong to the high-K calc-alkaline and shoshonite series (Fig. 2a). In the $(K_2O + Na_2O)–SiO_2$ classification diagram, data points of the granitoids of the Kibera Massif fall in the granite and granodiorite fields, except for monzonite from enclaves in the granites, while the rocks of the Kuekvun Massif plot in the monzonite, quartz monzonite, granodiorite, and granite fields; granite pebbles correspond to granodiorite and granite (Fig. 2b). The granitoids of the Kibera Massif and pebble are dominated by the calc-alkaline rocks, while the rocks of the Kuekvun Massif correspond mainly to both the calc-alkaline and subalkaline series.

According to the classification (Frost et al., 2001), the rocks of the Kibera Massif are mainly ascribed to the magnesian (Fe* = FeO_{tot}/FeO_{tot} + MgO) = 0.70–0.85), calcic and alkali-calcic, metaluminous to peraluminous (aluminum saturation index ASI > 1.0) granites (Fig. 3). The granitoids of the Kuekvun Massif correspond to the magnesian and ferroan varieties (Fe* = 0.75–0.90), alkali-calcic and calc-alkaline series, low-, moderate-, and partially peraluminous rocks (Fig. 3). Granite pebble differs from granites of the Kibera Massif (Tibilov et al., 1986) in very low Fe* = 0.43–0.61 (Fig. 3a), although their composition points fall also in the field of magnesian granites. They, as the granitoids of the Kibera Massif, are ascribed to the calcic and alkali-calcic rocks, but differ in the lower aluminum saturation index, plotting exclusively in the field of metaluminous granites (Figs. 3 b, 3c).

It is seen in the TiO_2, MgO, CaO, FeO_{tot}, Al_2O_3–SiO_2 diagrams that data points of the granitoids from the Kibera, Kuekvun massifs and conglomerate pebble define almost linear trends showing an increase of all these oxides with SiO_2 increase. Granite of the pebble has slightly lower Al_2O_3 and FeO_{tot} contents, and higher MgO at similar SiO_2 content (Fig. 4a). In the Na_2O, $K_2O–SiO_2$ diagram, data points of the granitoids show unsystematic variations (Fig. 4a).

In the rocks of the Kibera and Kuekvun massifs, an increase of Rb content is accompanied by the clear decrease of Sr content, which agrees with a trend of fractional crystallization (Cocherie, 1986) (Fig. 4b). A simultaneous decrease of Ba and Sr contents in the granitoids suggests fractionation of plagioclase and K-feldspar (Fig. 4b). Covariations of TiO_2 and Zr in the granitoids of both the massifs indicate fractionation of hornblende and biotite, and, to lesser extent, magnetite and titanite, while a decrease of $(La/Yb)_n$ and La content points to the fractionation of monazite and allanite (Fig. 4b). The latter is widespread in the rocks of the massifs, but monazite was not found in the polished thin sections. Data points of granite pebbles in the TiO_2–Zr and (La/Yb)n–La diagrams follows the same trends as granitoids of both the massifs, and are clustered separately in the Sr–Rb and Ba–Sr diagrams (Fig. 4b).

The chondrite-normalized fractionated REE patterns for granodiorite and granite from the Kibera Massif show LREE enrichment and HREE depletion, and clearly expressed negative Eu-anomaly (La_N/Yb_N = 10.10–17.95; Eu/Eu* = 0.54–0.72) (Fig. 5a). Similar REE patterns are typical of monzonite from melanocratic enclaves in granites (La_N/Yb_N = 12.41; Eu/Eu* = 0.70). The REE distribution patterns of granodiorite and granite pebble are

Table 1. Major (wt %) and trace (ppm) elements of representative varieties of the granitoids of the Kibera and Kuekvun massifs, and granite pebble at the base of the Lower Carboniferous sediments

Component	1	2	3	4	5	6	7	8	9	10
	Sample number									
	K-10-55	K-10-75	K-10-86	K-10-53	K-10-67	K-10-54	K-10-52	K-10-61	K-10-68	K-10-71
SiO_2	67.37	67.74	67.34	67.58	67.98	68.54	68.65	68.95	68.32	68.19
TiO_2	0.37	0.39	0.41	0.38	0.34	0.54	0.40	0.33	0.37	0.31
Al_2O_3	14.66	14.93	14.72	15.03	15.06	14.18	14.36	14.16	14.40	14.80
FeO	2.62	1.83	2.66	2.08	1.80	2.05	2.23	1.36	2.05	1.80
Fe_2O_3	1.32	2.49	1.88	2.09	1.97	2.04	1.79	2.19	1.90	1.83
MnO	0.09	0.07	0.07	0.073	0.074	0.12	0.076	0.06	0.08	0.07
MgO	1.25	1.14	1.40	1.25	1.19	1.36	1.25	1.07	1.22	1.08
CaO	3.08	3.29	2.48	1.92	2.50	2.32	2.82	3.11	2.96	3.31
Na_2O	3.45	3.52	3.71	2.80	3.83	3.74	3.77	3.42	3.67	3.87
K_2O	4.03	3.13	3.42	4.09	3.65	3.55	3.34	3.68	3.43	3.33
P_2O_5	0.14	0.17	0.23	0.158	0.141	0.19	0.167	0.15	0.16	0.13
L.O.I.	1.33	1.11	1.37	2.30	1.27	1.14	0.90	1.36	1.22	1.07
Total	99.70	99.80	99.70	99.54	99.80	99.77	99.75	99.83	99.77	99.79
V	51	64	77	54	53	66	57	43	52	54
Cr	27	14	25	12	12	20	32	9	10	20
Co	6	7	6	6	7	8	6	4	7	6
Ni	25	10	21	14	14	20	15	9	17	12
Ga	15.8	18.0	17.1	16.1	16.1	16.1	16.6	16.7	17.4	17.0
Rb	168	134	156	223	157	135	126	150	159	182
Sr	349	375	364	280	511	358	238	333	442	346
Y	15	18	21	18.7	15.2	20.3	17.6	15	17	19
Zr	148	164	306	156	144	190	153	147	154	166
Nb	12.4	11.9	14.7	13.0	11.8	14.9	16.3	12.2	13.3	12.8
Cs	4.0	4.1	3.9	6.7	3.6	3	3.1	2.9	3.4	5.7
Ba	706	671	623	606	462	637	360	815	564	463
Hf	4.4	4.6	7.0	4.8	4.4	4.8	4.6	4.5	4.5	4.3
Ta	0.9	0.9	1.2	1.1	0.83	1.4	1.2	0.9	0.9	1.1
Pb	24.6	27.0	23.4	14.4	17	22.1	12	20.9	19.6	25.1
Th	30.1	18.5	28.8	28	28	28.2	26.7	16.8	29.2	26.2
U	1.4	1.5	3.3	2.2	2.2	2.1	3.2	1.2	1.2	4.8
La	37.63	31.55	52.6	46.8	33.4	48.6	42.2	33.11	45.91	33.65
Ce	69.31	64.50	95.8	101	67.4	84.2	74.0	64.60	85.14	57.56
Pr	7.75	7.09	11.2	10.1	7.1	9.7	9.3	6.81	9.13	7.46
Nd	27.18	25.76	39.1	35.0	26.0	33.3	33.2	24.10	31.93	26.78
Sm	4.39	4.75	6.4	5.6	4.5	5.5	5.3	4.14	5.12	4.62
Eu	0.77	0.86	1.2	0.95	0.80	1.0	0.80	0.69	0.87	0.96
Gd	3.52	4.23	4.7	4.2	3.7	4.0	4.3	3.54	4.23	3.65
Tb	0.50	0.62	0.68	0.61	0.51	0.58	0.60	0.51	0.60	0.52
Dy	2.87	3.52	3.7	3.2	2.9	3.3	3.4	2.87	3.21	2.97
Ho	0.58	0.67	0.71	0.65	0.56	0.67	0.64	0.57	0.63	0.59
Er	1.65	1.96	2.1	1.8	1.7	2.0	1.9	1.69	1.88	1.78
Tm	0.26	0.29	0.30	0.26	0.25	0.28	0.28	0.26	0.28	0.26
Yb	1.80	2.02	2.1	1.8	1.8	1.9	2.0	1.75	1.95	1.79
Lu	0.27	0.29	0.32	0.28	0.27	0.30	0.31	0.27	0.30	0.28
La/Yb	15.01	11.21	17.83	18.21	13.47	17.95	15.26	13.60	16.91	13.45
Eu/Eu*	0.60	0.59	0.69	0.60	0.60	0.63	0.52	0.55	0.57	0.72

Table 1. (Contd.)

Component	11	12	13	14	15	16	17	18	19	20
	Sample number									
	K-10-79	K-10-80	K-10-81	K-10-7	K-10-9	K-10-77	K-10-78	K-10-97	K-10-73	K-10-76
SiO_2	68.21	68.29	69.57	69.07	70.36	69.77	69.9	70.9	70.9	71.06
TiO_2	0.36	0.36	0.30	0.32	0.32	0.34	0.31	0.27	0.3	0.26
Al_2O_3	14.81	15.05	14.33	14.25	13.70	14.2	14.81	13.93	13.8	13.75
FeO	1.4	2.34	1.54	1.98	1.98	1.87	1.62	0.54	1.44	1.04
Fe_2O_3	2.72	1.66	1.97	1.16	1.54	2.01	2.06	2.71	1.3	2.27
MnO	0.07	0.064	0.06	0.06	0.072	0.066	0.055	0.054	0.06	0.06
MgO	1.16	1.18	0.88	1.07	1.14	1.14	1.11	0.93	1.04	0.84
CaO	2.91	2.20	2.76	2.45	2.91	2.50	1.43	2.25	2.310	2.44
Na_2O	3.59	3.85	3.53	3.09	3.33	3.27	3.26	3.3	3.8	3.42
K_2O	3.51	3.38	3.84	5.01	3.23	3.54	3.86	3.93	3.0	3.8
P_2O_5	0.15	0.153	0.14	0.14	0.143	0.135	0.142	0.125	0.10	0.13
L.O.I.	0.96	1.2	0.86	1.18	1.05	0.94	1.26	0.98	1.2	0.81
Total	99.85	99.72	99.78	99.77	99.78	99.78	99.82	99.92	99.2	99.87
V	48	50	56	46	51	52	52	39	40	44
Cr	19	12	8	10	15	21	17	9	17	9
Co	8	5	6	5	6	6	6	5	4	5
Ni	13	13	9	12	13	15	12	9	15	11
Ga	16.2	17.2	18.3	13.9	16.6	16.6	17.5	15.8	14.2	14.0
Rb	132	147	155	189	172	124	150	174	120	166
Sr	402	341	371	332	379	386	396	291	203	278
Y	16	20	19	14	16	17	22	15	14	16
Zr	135	168	146	125	173	137	175	151	147	137
Nb	10.8	14.1	9.6	11.0	13.1	10.9	12.3	10.3	8.2	9.4
Cs	3.9	2.2	4.4	22.4	4.3	4.5	5.4	7.5	2.5	6.5
Ba	768	684	844	1229	419.0	749	994	788	770	787
Hf	4.0	5.4	4.3	4.1	4.9	4.1	4.3	4.5	3.6	4.3
Ta	0.8	1.4	1.0	0.9	1.0	0.8	1.1	0.8	0.7	1.0
Pb	27.3	27.9	23.7	22.9	20.7	26.1	23.8	40.9	15.1	30.3
Th	17.0	23.0	17.2	19.1	24.1	17.9	23.0	20.1	19.9	21.3
U	2.4	2.1	0.9	1.6	2.9	1.5	1.8	2.2	0.7	2.8
La	24.76	35.7	31.65	28.11	29.7	31.9	37.1	28.9	27.09	34.35
Ce	52.35	73.1	57.04	53.61	64.5	66.5	72.6	58.9	47.61	68.52
Pr	5.68	7.7	6.56	6.25	6.8	7.1	7.9	6.2	5.45	6.98
Nd	21.12	27.3	23.62	22.39	24.9	26.0	28.5	22.8	19.37	24.66
Sm	3.94	4.8	4.33	3.81	4.5	4.5	5.2	4.1	3.46	4.03
Eu	0.76	0.79	0.89	0.76	0.79	0.82	0.94	0.68	0.70	0.65
Gd	3.52	4.0	3.83	3.07	3.6	4.0	4.3	3.5	2.77	3.32
Tb	0.52	0.57	0.56	0.42	0.53	0.57	0.63	0.5	0.41	0.49
Dy	2.96	3.4	3.18	2.43	3.0	3.3	3.6	2.8	2.31	2.70
Ho	0.59	0.69	0.65	0.48	0.59	0.63	0.72	0.5	0.45	0.52
Er	1.74	2.0	1.88	1.39	1.8	1.9	2.1	1.5	1.35	1.59
Tm	0.25	0.30	0.27	0.20	0.26	0.27	0.29	0.22	0.19	0.23
Yb	1.76	2.1	1.86	1.43	1.8	1.9	1.9	1.6	1.21	1.62
Lu	0.28	0.32	0.28	0.22	0.29	0.28	0.27	0.23	0.18	0.24
La/Yb	10.10	12.16	12.23	14.07	11.55	11.94	14.12	12.95	16.06	15.18
Eu/Eu*	0.62	0.55	0.67	0.68	0.60	0.59	0.61	0.55	0.69	0.54

Table 1. (Contd.)

Component	21	22	23	24	25	26	27	28	29	30
	Sample number									
	K-10-84	K-10-89	K-10-91	K-10-69	K-10-85	K-10-83	K-10-70	K-10-74	K-10-92	K-10-199
SiO_2	72.27	71.27	70.19	74.34	74.73	74.26	74.92	76.27	55.95	56.01
TiO_2	0.27	0.32	0.30	0.06	0.07	0.06	0.07	0.10	0.50	1.04
Al_2O_3	12.79	14.08	14.27	14.56	14.15	14.86	13.60	12.55	17.08	16.33
FeO	1.62	0.86	1.51	0.51	0.4	1.80	0.55	0.47	1.08	3.77
Fe_2O_3	1.69	2.25	1.75	0.57	0.53	0.43	0.34	0.91	2.84	4.50
MnO	0.06	0.041	0.06	0.05	0.025	0.07	0.020	0.018	0.30	0.113
MgO	1.05	1.03	1.22	0.17	0.17	0.18	0.14	0.22	1.05	2.58
CaO	2.17	0.89	1.99	0.38	0.31	0.44	0.51	0.77	6.76	6.45
Na_2O	2.96	3.23	3.24	3.72	3.68	4.03	4.28	2.93	5.51	3.22
K_2O	3.71	4.47	3.92	4.43	5.26	4.04	4.66	5.38	3.29	3.86
P_2O_5	0.13	0.135	0.13	0.10	0.095	0.17	0.1	0.029	0.23	0.683
L.O.I.	1.09	1.31	1.26	1.06	0.56	0.75	0.75	0.38	5.3	0.92
Total	99.81	99.89	99.84	99.95	99.96	101.09	99.94	100.03	99.88	99.48
V	44	42	41	6	9	3	6	18	71	–
Cr	19	9	14	6	11	5	18	29	5	–
Co	8	4	5	1	0	1	2	2	14	–
Ni	13	8	11	5		6	13	18	11	–
Ga	13.3	16.5	17.0	21.5	15.5	14.8	18.3	15.2	18.0	–
Rb	149	187	162	368	275	286	231	177	222	–
Sr	236	243	393	36	38	72	106	107	355	–
Y	14	12	16	20	13	12	11	10	23	–
Zr	139	139	145	42	33	33	42	78	228	–
Nb	9.2	14.0	11.7	16.7	18.8	11.0	14.2	6.4	14.3	–
Cs	3.6	6.8	5.1	16.3	10.3	51.2	6.0	3.7	14.5	–
Ba	361	859	874	39.2	109.0	128	115	167	565	–
Hf	4.5	4.2	4.3	2.6	2.0	1.5	2.3	3.3	5.5	–
Ta	0.8	1.0	0.8	3.6	2.9	2.9	3.2	0.9	1.2	–
Pb	31.4	26.9	24.3	39.6	36.9	42.3	49.4	37.4	8.7	–
Th	25.2	18.1	27.8	8.6	8.4	3.3	8.6	23.7	21.3	–
U	7.4	2.0	2.1	1.6	1.6	3.8	8.4	3.5	5.3	–
La	31.97	32.9	37.61	6.78	7.4	5.31	9.4	11.8	35.49	–
Ce	61.18	64.6	74.03	14.64	16.0	11.38	17.6	26.1	65.72	–
Pr	6.39	6.9	7.98	1.70	1.8	1.25	2.0	2.7	7.42	–
Nd	21.74	25.0	27.84	5.72	6.6	4.51	6.7	9.7	26.74	–
Sm	3.48	4.3	4.81	1.76	1.8	1.28	1.6	1.9	4.71	–
Eu	0.59	0.75	0.80	0.06	0.06	0.24	0.12	0.28	0.98	–
Gd	2.75	3.3	3.91	2.26	1.9	1.56	1.7	1.7	3.87	–
Tb	0.39	0.5	0.57	0.49	0.40	0.32	0.29	0.27	0.55	–
Dy	2.21	2.6	3.09	3.19	2.6	2.11	1.9	1.6	3.34	–
Ho	0.45	0.5	0.59	0.64	0.50	0.37	0.35	0.33	0.70	–
Er	1.30	1.4	1.68	1.95	1.5	1.03	1.0	1.0	2.15	–
Tm	0.20	0.20	0.25	0.31	0.23	0.15	0.16	0.16	0.29	–
Yb	1.43	1.4	1.76	2.19	1.6	0.99	1.1	1.2	2.05	–
Lu	0.22	0.21	0.26	0.31	0.22	0.13	0.16	0.18	0.34	–
La/Yb	16.03	16.82	15.29	2.22	3.30	3.84	6.17	7.03	12.41	
Eu/Eu*	0.58	0.60	0.57	0.50	0.10	0.52	0.22	0.47	0.70	

Table 1. (Contd.)

Component	31	32	33	34	35	36	37	38	39	40
	Sample number									
	K-10-198	K-10-189	K-10-194	K-10-217	K-10-218	K-10-185	K-10-186	K-10-196	K-10-25	K-10-29/5
SiO_2	56.44	63.51	65.27	70.29	72.09	75.65	73.43	74.14	63.90	64.83
TiO_2	1.02	0.40	0.46	0.25	0.20	0.10	0.13	0.15	0.34	0.36
Al_2O_3	15.99	16.57	15.5	14.05	13.69	13.10	14.03	13.25	14.18	13.99
FeO	3.63	2.3	2.52	1.08	0.93	0.36	0.36	0.54	1.78	1.07
Fe_2O_3	4.55	1.80	2.31	2.13	1.70	0.99	1.29	1.18	0.68	1.38
MnO	0.11	0.06	0.07	0.08	0.07	0.04	0.04	0.05	0.01	0.01
MgO	2.45	0.99	1.43	0.79	0.50	0.14	0.20	0.28	1.73	1.60
CaO	6.34	3.60	3.52	2.46	2.09	0.98	1.36	1.07	5.17	5.05
Na_2O	3.19	3.24	3.13	2.82	2.92	3.1	3.25	2.87	2.78	4.61
K_2O	4.25	5.83	4.26	4.93	4.71	4.79	5.02	5.51	4.13	2.20
P_2O_5	0.71	0.25	0.30	0.14	0.10	0.02	0.03	0.04	0.16	0.18
L.O.I.	0.86	0.78	1.2	1.01	0.65	0.44	0.69	0.94	4.94	4.62
Total	99.52	99.32	99.96	100.03	99.65	99.70	99.83	100.01	99.79	99.90
V	136	60	83	29	20	4	12	13	57	–
Cr	10	9	5	14	47	4	3	7	6	–
Co	15	6	10	3	3	1	1	2	2	–
Ni	11	10	7	11	41	3	bdl	bdl	bdl	–
Ga	19.8	18.2	18.3	14.5	14.4	15.3	15.9	15.2	11.0	–
Rb	92	129	125	148	136	243	247	232	86	–
Sr	1589	816	530	401	289	88	109	130	76	–
Y	45	34	48	20	19	51	41	26	5	–
Zr	375	181	355	120	56	102	106	114	124	–
Nb	18.1	16.7	19.4	16.0	15.4	17.6	18.1	12.4	7.8	–
Cs	2.9	4.1	3.0	3.4	2.1	3.1	7.3	3.9	5.6	–
Ba	2331	2105	1202	1094	641	276	365	426	929	–
Hf	7.7	5.4	7.5	4.2	2.4	4.8	4.1	4.0	3.9	–
Ta	1.2	1.3	1.6	1.3	1.3	1.1	1.2	1.4	0.6	–
Pb	20.1	22.6	19.3	20.3	14.1	42.3	33.6	29.9	16.2	–
Th	36.9	42.1	44.0	24.5	21.1	19.9	19.7	31.0	14.5	–
U	4.1	3.8	2.5	3.2	2.3	3.4	3.3	3.1	1.0	–
La	106.26	131.75	148.75	40.40	34.28	7.92	25.48	47.56	15.60	–
Ce	229.43	240.33	250.85	73.85	60.89	28.06	65.11	91.01	32.94	–
Pr	29.86	25.49	31.16	8.14	7.19	2.00	5.89	10.74	3.54	–
Nd	111.94	91.21	105.34	29.10	25.46	7.62	20.80	37.57	12.78	–
Sm	19.73	14.32	16.85	4.78	4.20	2.11	3.89	6.99	1.90	–
Eu	4.46	2.41	2.99	0.91	0.77	0.35	0.45	0.58	0.35	–
Gd	13.03	10.39	11.81	3.64	3.14	4.06	4.01	5.86	1.28	–
Tb	1.70	1.44	1.64	0.56	0.49	0.89	0.71	0.86	0.17	–
Dy	8.49	7.23	8.63	3.22	2.81	7.31	5.36	4.51	0.87	–
Ho	1.51	1.38	1.59	0.67	0.61	1.77	1.28	0.87	0.16	–
Er	4.18	3.88	4.40	2.04	1.98	6.03	4.17	2.47	0.50	–
Tm	0.54	0.53	0.57	0.32	0.32	0.94	0.66	0.37	0.08	–
Yb	3.44	3.45	3.61	2.21	2.36	6.63	4.39	2.52	0.58	–
Lu	0.49	0.45	0.49	0.33	0.36	0.95	0.66	0.37	0.10	–
La/Yb	22.15	27.41	29.52	13.09	10.40	0.86	4.16	13.52	19.27	–
Eu/Eu*	0.85	0.60	0.65	0.67	0.65	0.36	0.35	0.28	0.68	

Table 1. (Contd.)

Component	41	42	43	44	45	46	47	48		
	Sample number									
	K-10-29/12	K-10-29/11	K-10-27	K-10-29/2	K-10-29/1	K-10-29/7	K-10-29/14	K-10-29/9		
SiO_2	65.54	69.79	70.66	70.82	72.13	72.12	72.25	72.76		
TiO_2	0.40	0.38	0.20	0.16	0.36	0.38	0.21	0.36		
Al_2O_3	14.4	12.94	13.66	12.63	12.71	13.10	12.49	12.77		
FeO	0.96	0.1	0.22	0.31	0.27	0.12	0.22	0.12		
Fe_2O_3	1.80	1.66	1.49	1.18	1.21	1.44	1.34	1.27		
MnO	0.01	<0.01	0.01	0.01	<0.01	<0.01	<0.01	<0.01		
MgO	1.94	2.08	1.12	1.10	1.58	1.58	0.91	1.49		
CaO	3.73	2.37	2.40	3.23	1.57	1.18	2.48	1.27		
Na_2O	4.72	4.58	2.57	5.52	4.86	5.13	4.92	4.89		
K_2O	2.64	2.88	5.16	2.11	2.91	2.90	2.81	3.02		
P_2O_5	0.19	0.20	0.07	0.04	0.18	0.18	0.08	0.17		
L.O.I.	3.57	3.01	2.43	2.88	2.16	1.86	2.27	1.86		
Total	99.90	99.99	99.98	99.99	99.94	99.99	99.98	99.98		
V	60	46	31	21	–	35	29	32		
Cr	21	12	7	10	–	10	17	14		
Co	bdl	2	3	2	–	5	bdl	3		
Ni	11	12	bdl	13	–	13	10	14		
Ga	10.3	11.3	11.1	10.9	–	11.3	10.3	10.3		
Rb	106	107	94	112	–	107	106	106		
Sr	61	85	41	66	–	85	61	61		
Y	8	8	6	18	–	8	8	8		
Zr	182	149	92	109	–	149	182	182		
Nb	10.4	10.1	8.1	9.7	–	10.1	10.4	10.4		
Cs	6.6	6.3	5.0	3.2	–	6.3	6.6	6.6		
Ba	1861	1792	1119	1351	–	1792	1861	1861		
Hf	4.6	3.8	3.4	3.2	–	3.8	4.6	4.6		
Ta	1.0	0.9	0.9	1.5	–	0.9	1.0	1.0		
Pb	44.8	48.8	16.8	26.2	–	48.8	44.8	44.8		
Th	21.1	26.0	16.4	23.6	–	26.0	21.1	21.1		
U	2.4	2.5	1.2	1.9	–	2.5	2.4	2.4		
La	33.88	30.58	14.58	29.88	–	30.58	33.88	33.88		
Ce	68.15	63.40	32.29	52.61	–	63.40	68.15	68.15		
Pr	7.28	6.78	3.57	5.30	–	6.78	7.28	7.28		
Nd	25.71	23.95	13.23	18.21	–	23.95	25.71	25.71		
Sm	4.15	3.87	2.07	3.45	–	3.87	4.15	4.15		
Eu	0.60	0.58	0.33	0.31	–	0.58	0.60	0.60		
Gd	2.67	2.67	1.42	3.07	–	2.67	2.67	2.67		
Tb	0.34	0.33	0.20	0.49	–	0.33	0.34	0.34		
Dy	1.55	1.65	0.97	2.97	–	1.65	1.55	1.55		
Ho	0.28	0.30	0.21	0.58	–	0.30	0.28	0.28		
Er	0.83	0.89	0.59	1.79	–	0.89	0.83	0.83		
Tm	0.12	0.13	0.10	0.26	–	0.13	0.12	0.12		
Yb	0.85	0.86	0.70	1.70	–	0.86	0.85	0.85		
Lu	0.13	0.13	0.11	0.25	–	0.13	0.13	0.13		
La/Yb	28.58	25.38	14.83	12.61		25.38	28.58	28.58		
Eu/Eu*	0.55	0.55	0.59	0.29		0.55	0.55	0.55		

Kibera Massif: (1–13) granodiorite; (14–23) granite; (24–28) alaskite; (29) monzonite from enclave. Kuekvun Massif: (30, 31) monzonite; (32) quartz monzonite; (35) granodiorite; (34–36) granite; (37, 38) alaskite. Granitoid pebble: (39–42) granodiorite; (43–48) granite.

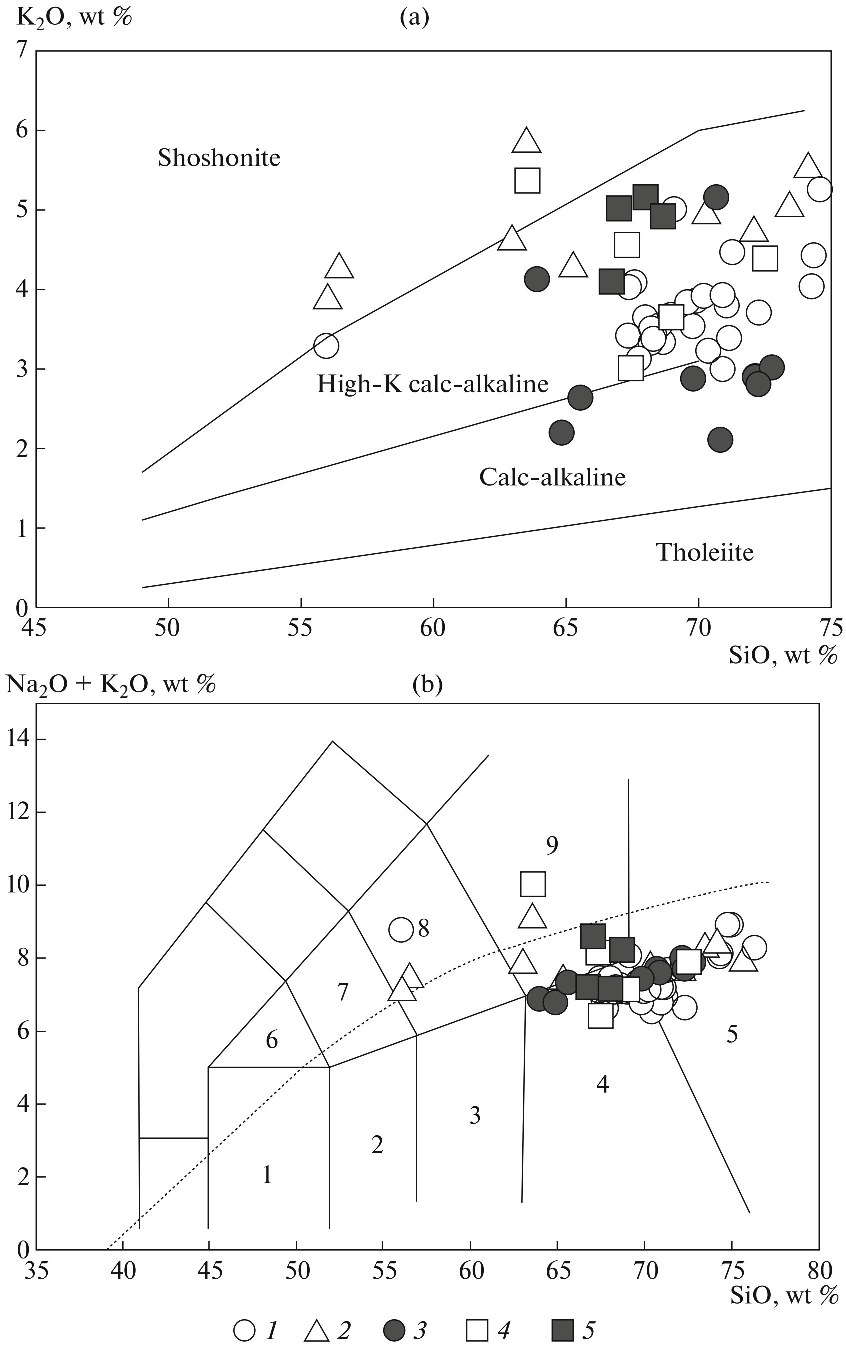

Fig. 2. Diagram K_2O–SiO_2 (Peccerilo and Taylor, 1976) (a) and ($Na_2O + K_2O$)–SiO_2 (Middlemost, 1994) (b) for granitoids of the Kibera and Kuekvun massifs and granite pebble from conglomerate at the base of the Lower Carboniferous rocks. (b): fields: (1) gabbro, (2) gabbrodiorite, (3) diorite, (4) granodiorite, (5) granite, (6) monzogabbro, (7) monzodiorite, (8) monzonite, (9) quartz monzonite. (*1, 2*) granitoids: (*1*) Kibera Massif, (*2*) Kuekvun Massif; (*3*) granite pebble from conglomerate at the base of the Lower Carboniferous rocks; (*4*) granite of the Kibera Massif (Tibilov et al., 1986); (*5*) granite pebble from conglomerate at the base of the Carboniferous rocks (Tibilov et al., 1986).

more fractionated, with clearly expressed negative Eu-anomaly (La_N/Yb_N = 12.61–28.58; Eu/Eu* = 0.28–0.68) (Fig. 5c). The REE distribution pattern in the alaskite differs from others in the nearly horizontal HREE distribution and the deeper negative Eu anomaly (La_N/Yb_N = 2.22–13.21; Eu/Eu* = 0.10–0.50) (Fig. 5a).

Monzonite, quartz monzonite, and granodiorite from the Kuekvun Massif have fractionated chondrite-normalized REE patterns with small negative Eu

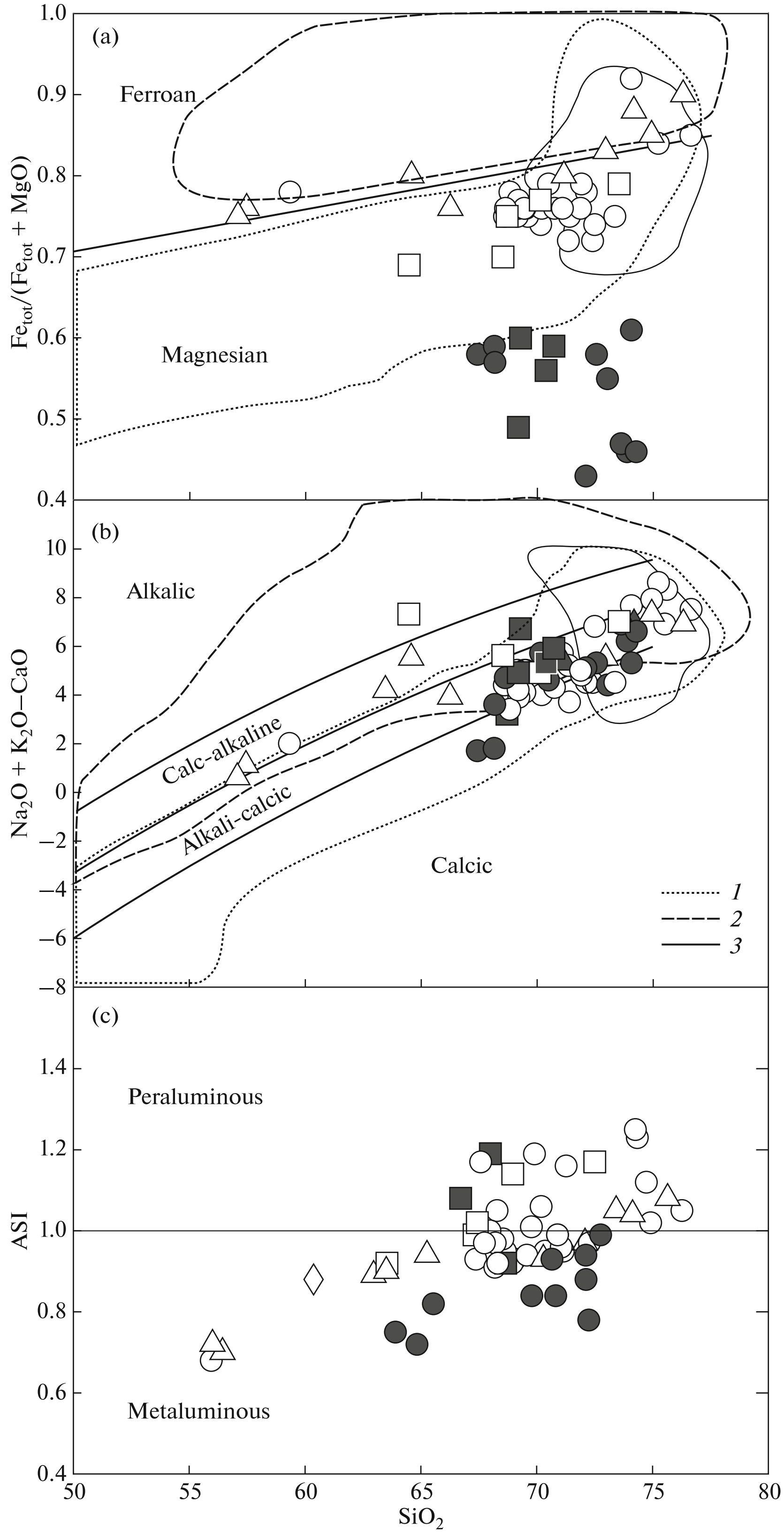

Fig. 3. Diagrams $Fe_{tot}/(Fe_{tot} + MgO)-SiO_2$ (a), $(Na_2O + K_2O)-(CaO-SiO_2)$ (b), ASI$-SiO_2$ (c) (Frost et al., 2001) for granitoids of the Kibera and Kuekvun massifs, and granite pebble from conglomerates at the base of the Lower Carboniferous rocks. Fields of granites in Figs. (a, b): (*1*) I-type Cordilleran, (*2*) A-type, (*3*) peraluminous leucogranite. Symbols are shown in Fig. 2.

anomaly (La_N/Yb_N = 12.41–27.41; Eu/Eu* = 0.60–0.85) (Fig. 5b). The granites have similar REE patterns, but the lower total REE abundance (La_N/Yb_N = 10.40–29.52; Eu/Eu* = 0.65–0.67) (Fig. 5b). The REE distribution of the alaskite, as those of granites from the Kibera Massif, differs in the similar enrichment in LREE and HREE and deeper negative Eu anomaly (La_N/Yb_N = 0.86–4.16; Eu/Eu* = 0.36–0.67) (Fig. 5b).

The spidergrams of granitoids of the Kibera and Kuekvun massifs are characterized by similar distribution (Figs. 6a, 6b). They are enriched in LILE relative to HFSE, and have positive anomalies of K, Pb, and negative anomalies of Ba, Sr, Nb, Ta, P, and Ti. The spidergrams of the pebble granites and granodiorites are identical to those of the granitoids of the Kibera Massif, but differ in the negative Rb anomaly and even deeper Sr anomaly (Fig. 5c).

The petrogeochemical types of the granitoids of the Kibera and Kuekvun massifs and pebble were determined using diagrams based on the major and trace elements (Fig. 7). In particular, in the FeO*/MgO – (Zr + Nb + Ce + Y) and Zr – 10^4Ga/Al (Whalen et al., 1987) diagrams with separation between I-, S- and A-types granites, data points of the granitoids fall in the fields of I- and S-type granites, including highly differentiated I-type granites (Fig. 7a) or unfractionated and fractionated granites of the M-, I-, and S-types (Fig. 7b). Only some compositions of granitoids with elevated content of Zr or sum of Zr + Nb + Ce + Y fall in the field of A-type granites (Figs. 7a, 7b). In the Nb–Sr diagram (Whalen et al., 1987), data points of all granitoids are grouped around average I-type granite (Fig. 7 c). In the (Al_2O_3 + CaO)/(FeO_{tot} + Na_2O + K_2O) and 100*(MgO + FeO + TiO_2)/SiO_2 diagrams (Sylvester, 1989), they are ascribed to the I-type granites, including highly differentiated granites (Fig. 7 d). In the P_2O_5–SiO_2 diagram, data points of all granitoids follow a trend typical of I-type granites, although the granitoids of the Kuekvun Massif define a steeper trend due to the higher contents of more mafic rock varieties (Fig. 7e). Most part of the granitoids also follow the trend typical of the I-type granites in the Pb–SiO_2 diagram, but most evolved varieties are grouped around trend of S-type granites (Fig. 7f).

In the Rb–(Y + Nb) and Y–Nb diagrams (Pearce et al., 1984; Pearce, 1996) (Fig. 8) applied to separate between granitoids of different geodynamic settings, data points of the granitoids of the Kibera and Kuekvun massifs and granitoids from conglomerate pebble at the base of the Carboniferous sequence fall in the boundary between the fields of the volcanic arc, syncollisional and within-plate granites. In the Rb–(Y + Nb) diagram (Fig. 8a), the majority of data points are overlapped by the field of postcollisional granites.

Sr–Nd–Pb ISOTOPE CHARACTERISTICS OF THE GRANITOIDS

The Sr, Nd, and Pb isotope compositions of the studied samples are shown in Table 2. The studies were undertaken for granite, granodiorite, alaskite, and enclave monzonite from the Kibera Massif, granodiorite and quartz monzodiorite from the Kuekvun Massif, as well as for granite pebble from conglomerate at the base of the Lower Carboniferous sediments.

Initial $^{143}Nd/^{144}Nd$ ratio in the studied granitoids varies within 0.512037–0.512134, which corresponds to εNd(T) varying in a narrow range from –0.95 to –2.83 (Table 2). With the growth of SiO_2 from enclave monzonite to granite and granodiorite of the Kuekvun and Kibera massifs, εNd(T) practically show no any variations and then sharply decreases from granite to alaskite through granite pebble.

Model, single-stage (TDM1) and two-stage (TDM2) ages of the granitoids from both the massifs and granite pebble are sufficiently close and correspond to the intervals of 1034–1148 and 1203–1300 Ma, which correspond to the Mesoproterozoic. The exception is the alaskite from the Kibera Massif, which has the older Paleoproterozoic single-stage model age (2218 Ma) and slightly older Mesoproterozoic two-stage age (1361 Ma) as compared to other granitoids.

The granitoids of both the massifs have relatively high initial $^{87}Sr/^{86}Sr$ from 0.705889 to 0.707845. The lowest values were found in the monzonite from enclaves in the Kibera Massif, while the highest values were determined in the granodiorite from the same massif. Granite pebble is sharply distinguished in extremely low initial $^{87}Sr/^{86}Sr$ (0.695045), which is determined by the elevated Rb/Sr ratio due to excess mobility of the system in micas.

Sr-Nd isotope data on the coeval Late Devonian–Early Carboniferous granitoids of the Yukon–Tanana terrane of Alaska (Ruks et al., 2006), which characterize the Late Paleozoic active margin of the North American continent, and Aptian–Albian granitoids of the Alyarmaut Uplift of West Chukotka (Fig. 1a) (Luchitskaya et al., 2010) are shown in Fig. 9 for comparison. The latters at present are the only isotopically–geochemically studied objects of the Chukotka region. The granitoids of the Yukon–Tanana terrane differ from the granitoids of the Kibera and Kuekvun massifs in the lower negative εNd(T) and older model ages (Fig. 9a), while the granitoids of the Alyarmaut Uplift have εNd(T) from –2.32 to –4.99, but the wider variations in initial $^{87}Sr/^{86}Sr$ (Fig. 9b) and close single-stage ages (1013–1389 Ma, excluding single values 1721 and 2140 Ma) (Luchitskaya et al., 2010).

The Pb isotope composition of the granitoids of the Kibera Massif varies in a wide range: $^{206}Pb/^{204}Pb$ = 18.8615–20.1301, $^{207}Pb/^{204}Pb$ = 15.6015–15.7134, $^{208}Pb/^{204}Pb$ = 38.4355–39.3947. The granitoids of the Kuekvun Massif are characterized by steadier isotope

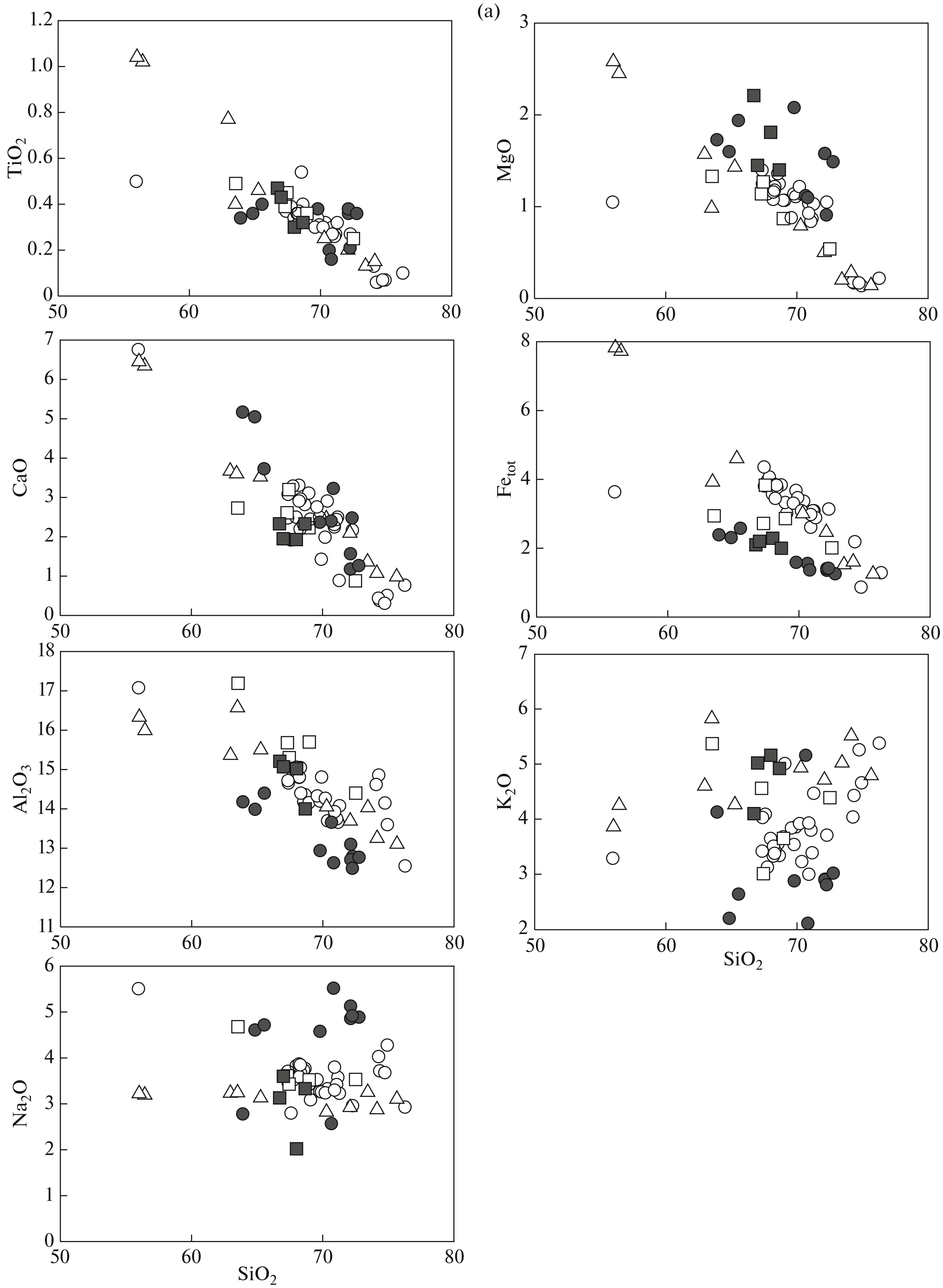

Fig. 4. Diagrams TiO_2, MgO, CaO, FeO_{tot}, Al_2O_3, K_2O, Na_2O-SiO_2 (a), and Sr–Rb, Ba–Sr, TiO_2–Zr, $(La/Yb)_N$–La (b) for the granitoids of the Kibera and Kuekvun massifs and granite pebble from conglomerate at the base of the Lower Carboniferous rocks. (PM) partial melting; (FC) fractional crystallization. Vectors showing the fractionation of minerals after (Li et al., 2012). Symbols are shown in Fig. 2.

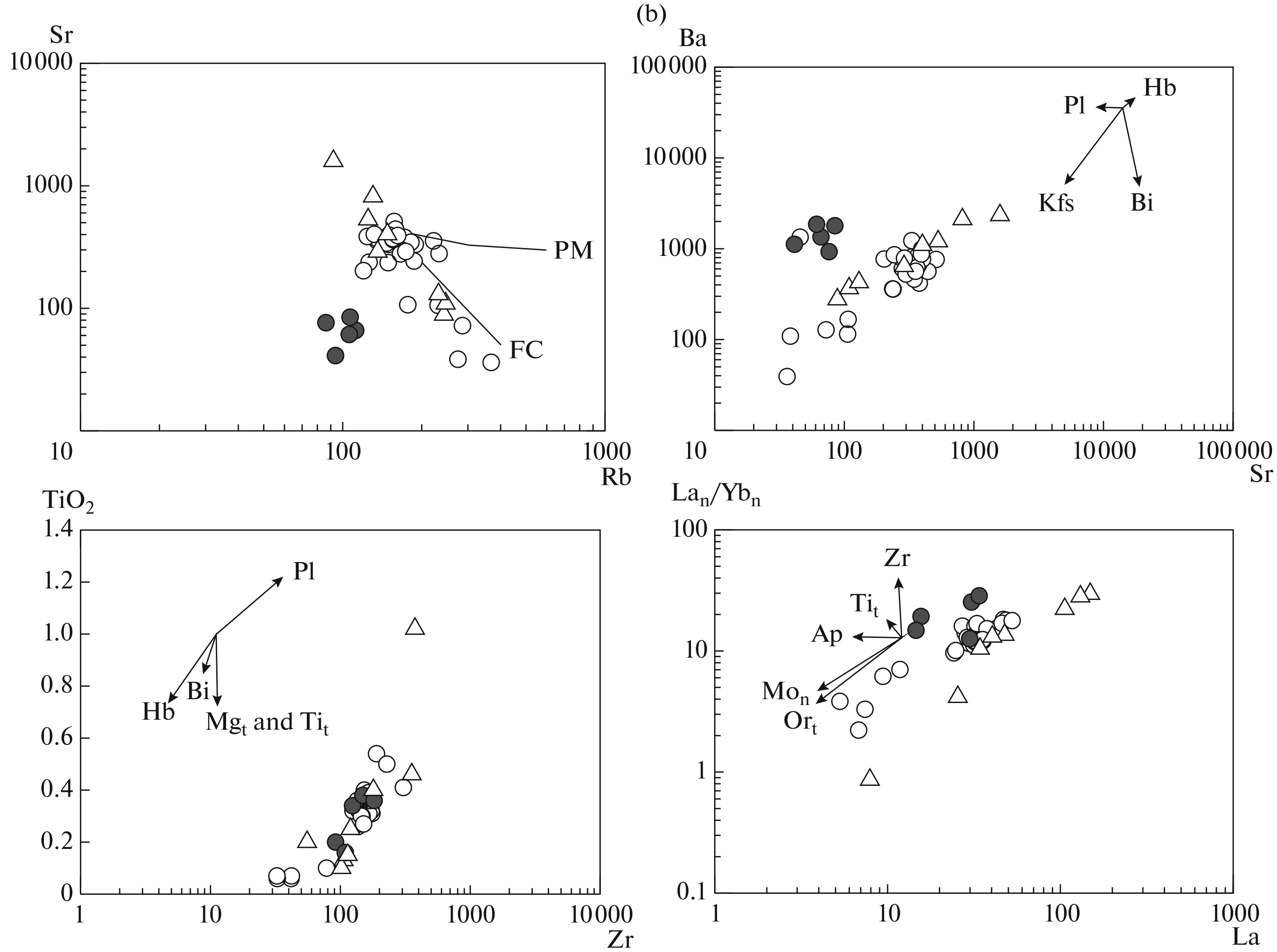

Fig. 4. (Contd.)

composition: $^{206}Pb/^{204}Pb$ = 19.0710–19.4393, $^{207}Pb/^{204}Pb$ = 15.6105–15.6425, $^{208}Pb/^{204}Pb$ = 39.5055–40.1312. In contrast, granite pebble has less radiogenic Pb composition: $^{206}Pb/^{204}Pb$ = 18.6909, $^{207}Pb/^{204}Pb$ = 15.6157, $^{208}Pb/^{204}Pb$ = 38.7637.

In the $^{207}Pb/^{204}Pb$–$^{206}Pb/^{204}Pb$ diagram, the values of Pb isotope ratios for the granitoids of both the massifs and granite pebble define a linear trend, which can be interpreted either according to isochron model, i.e., a slope of linear trend should reflect the age of lead accumulation if the U-Pb geochemical system of these granitoids remained undisturbed, or as a mixing curve of leads from different sources (Fig. 10a). Considering the obtained linear trend as isochron dependence, the slope corresponds to an age of 1133 ± 470 Ma, while MSWD is more than 100, and linear trend intersects a Stacey-Kramers Pb evolution curve at an age of 1440 Ma. In the $^{208}Pb/^{204}Pb$–$^{206}Pb/^{204}Pb$ diagram, the linear trend is preserved only for the granitoids of the Kibera Massif, except for alaskite sample, which at high $^{206}Pb/^{204}Pb$ (20.1301) ratios has low ratio of $^{208}Pb/^{204}Pb$ (38.4355) (Fig. 10 b). The granitoids of the Kuekvun Massif have wide $^{208}Pb/^{204}Pb$ variations at close $^{206}Pb/^{204}Pb$ ratios (Fig. 10b). Thus, the indicated features of Pb isotope composition suggest that the studied set of granitoid samples cannot be considered as an undisturbed homogenous U-Pb isotope system with common Th/U ratio, and the linear trend in the $^{207}Pb/^{204}Pb$–$^{206}Pb/^{204}Pb$ diagram, as secondary isochron corresponding to the formation time of the granitoids.

The $^{207}Pb/^{204}Pb$–$^{206}Pb/^{204}Pb$ diagram (Fig. 11) demonstrates the Pb isotope evolution curve of mantle, lower and upper crustal orogenic reservoirs, two-stage terrestrial Pb-isotope evolution curve (Stacey and Kramers, 1975), as well as the fields of the lower and upper crustal model sources, mature and primitive island arcs. Data points of the initial Pb isotope composition (calculated for age of 350 Ma) of granitoids of the Kibera and Kuekvun massifs and granite pebble fall in the Pb evolution curve of the orogenic reservoir. Exception is monzonite enclave from the Kibera Massif, data point of which is located between

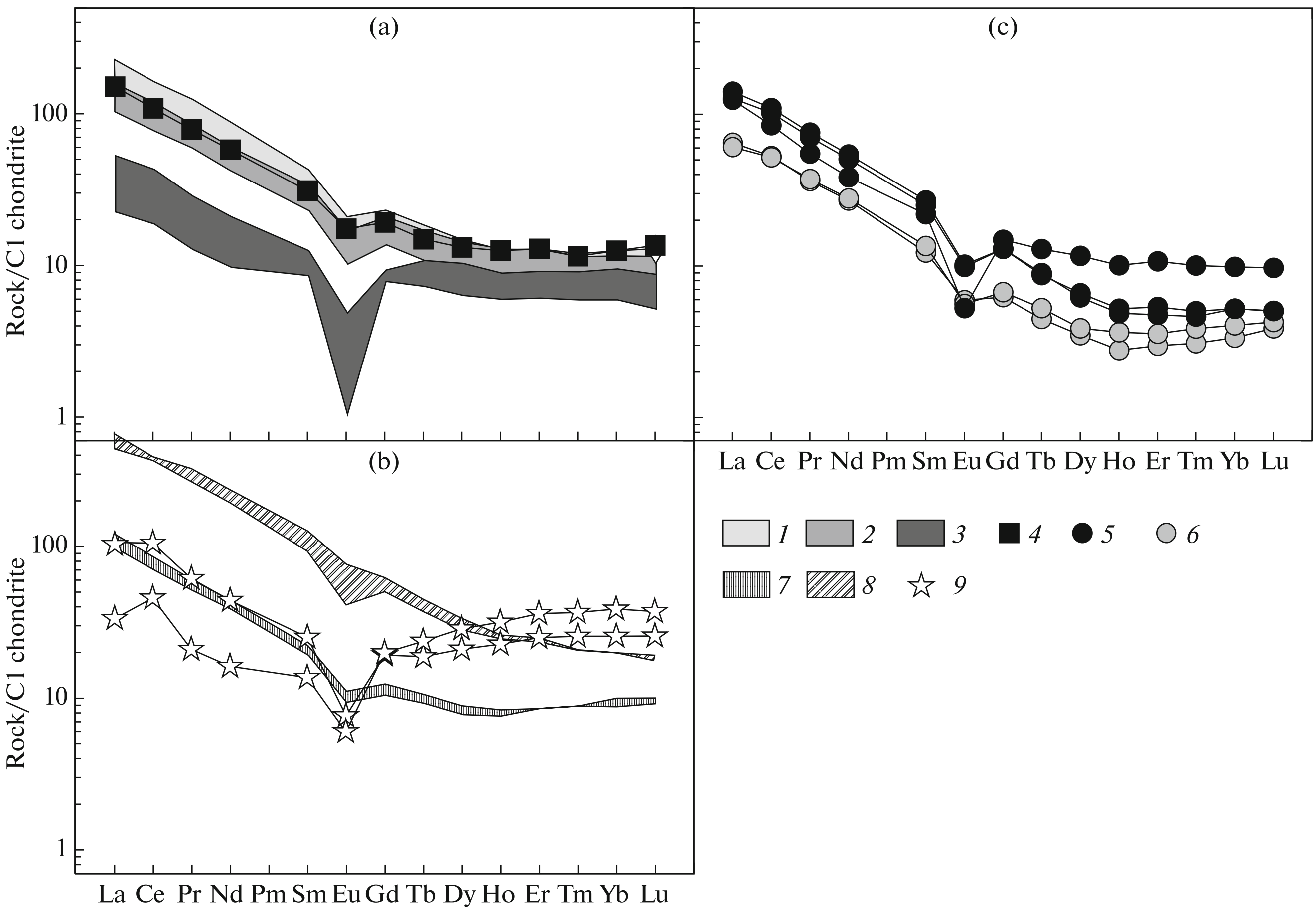

Fig. 5. Chondrite-normalized REE patterns for the granitoids of the Kibera (a) and Kuekvun massifs (b), granite pebble from conglomerate at the base of Carboniferous rocks (c). Chondrite C1 composition after (Sun and Donough, 1989). (*1–5*) granitoids of the Kibera Massif: fields: (*1*) granodiorite, (*2*) granite, (*3*) alaskite; (*4*) distribution in monzonites; (*5, 6*) distribution in granite pebble from conglomerates at the base of the Lower Carboniferous rocks: (*5*) granite, (*6*) granodiorite; (*7–9*) granitoids of the Kuekvun Massif: fields: (*7*) granite, (*8*) monzonite, quartz monzonite, granodiorite; (*9*) distribution of alaskites.

the evolution curves of the orogenic and upper crustal reservoirs. It is noteworthy that the data points of Pb isotope composition of the granitoids from both the massifs and granite pebble are mainly confined to the mature island arc field (Fig. 11). Data points corresponding in composition to monzonite from enclaves in the granites of the Kibera Massif and quartz monzodiorite from the Kuekvun Massif fall in the fields of the upper and lower crustal sources, respectively.

Hf ISOTOPE COMPOSITION OF ZIRCONS

Geochronological studies of the granitoids of the Kibera and Kuekvun massifs reported in (Katkov et al., 2013; Luchitskaya et al., 2015) were accompanied by the analysis of Hf isotope composition of zircon from two granite samples of the Kibera Massif (samples K-10-9, K-10-73) with ages of 357 ± 4 and 352 ± 4 Ma and granite pebble from conglomerates at the base of the Lower Carboniferous sequences (sample K-10-27) with an age of 359 ± 3 Ma. Results of studies of the Hf isotope composition are presented in Table 3.

Analysis of the Lu–Hf isotope system of granites from the Kibera Massif revealed a wide scatter of $^{176}Hf/^{177}Hf$ ratio within 0.282721–0.283418 (Fig. 12a), which corresponds to εHf variations from +16.7 to –5.2. Intervals of these values for zircons from granite pebble are slightly lower 0.282415–0.283683, i.e. εHf is characterized by only positive values from +16.7 to +6.5 (Fig. 12b). Single-stage model ages (T_{DM}) for zircons from granites of the Kibera Massif and pebbles reveal practically similar scatter, coinciding with an age of granites from 300 to 740 and to 720 Ma, respectively. At the same time, maximum two-stage model ages ($T_{DM}C$) are different: – 1.57 and 0.88 Ga, respectively. Most part of data points with positive εHf in the diagram εHf–age are plotted between curves of CHUR (εHf = 0) and DM (Fig. 12b), which indicates a certain mantle contribution during formation of the granitoids. Negative εHf typical of only zircons from granites of the Kibera Massif (sample K-10-9) can

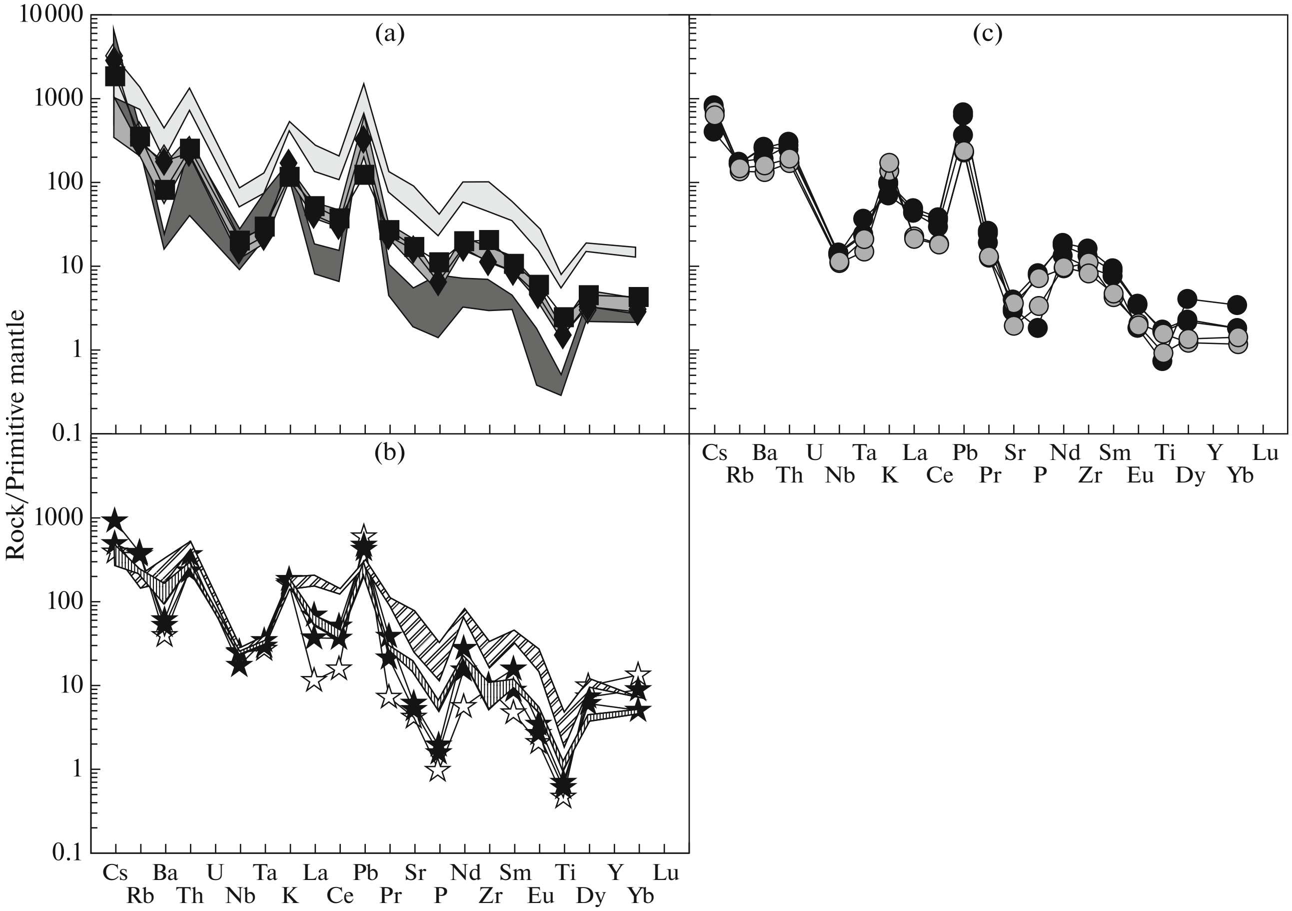

Fig. 6. Spidergrams for granitoids of the Kibera (a) and Kuekvun massifs (b), granite pebble from conglomerate at the base of the Lower Carboniferous rocks (c)/ Composition of primitive mantle after (Sun and Donough, 1989). Symbols are shown in Fig. 5.

reflect the presence of ancient (no older than Mesoproterozoic) crustal material in the protolith, melting of which produced granitoid magmas.

DISCUSSION

Petrographic composition, petrogeochemical, and isotope characteristics of the granitoids of the Kibera and Kuekvun massifs and granite pebble from the base of the Lower Carboniferous sequence indicate their affiliation to the Cordilleran I-type granite (Chappell and White, 1992; Frost et al., 2001). Some granitoids have peraluminous ASI index (Fig. 3c), which previously was considered as characteristic feature of S-type granites. However, it was recently shown (Clemens et al., 2011; Chappell et al., 2012) that I-type granite series contain peraluminous varieties together with more mafic metaluminous rocks. In the $(Al_2O_3 + CaO)/(FeO_{tot} + Na_2O + K_2O)$ versus $100^*(MgO + FeO + TiO_2)/SiO_2$ diagram, some granites of the Kibera and Kuekvun massifs correspond to the highly differentiated I-type granites. The same is seen in the diagram Zr–10^4Ga/Al (Figs. 7a, 7d). Sufficiently high Zr contents of sum of Zr + Nb + Ce + Y typical of A-type granites and observed in some granitoids of the Kuekvun Massif make it impossible, however, to ascribe them to the granites of this type, because granitoids of this massif are not purely ferroan and alkaline rocks, as should be expected for A-type granites (Whalen et al., 1987; Frost et al., 2001 etc.). The Nb and Sr contents in the granitoids of both the massifs and granite pebble also indicate their clear difference from A-type granites (Fig. 7c).

As known, the formation of I-type granites is related to partial melting of older metamagmatic rocks (Chappel and White, 1992). These rocks could be metabasites corresponding to the basaltic layer of oceanic crust and/or lower crust, or intermediate rocks containing biotite and hornblende–andesite, or tonalite corresponding to the bulk composition of crust or average crust. The most representative experimental data on metabasite melting are summarized in (Turkina, 2000; Kruk, 2015). It is shown that dehydration or hydrous melting of metabasites within the range of 950–1050°C and 3–20 kbar yields Na melts enriched in Ca and femic components and corre-

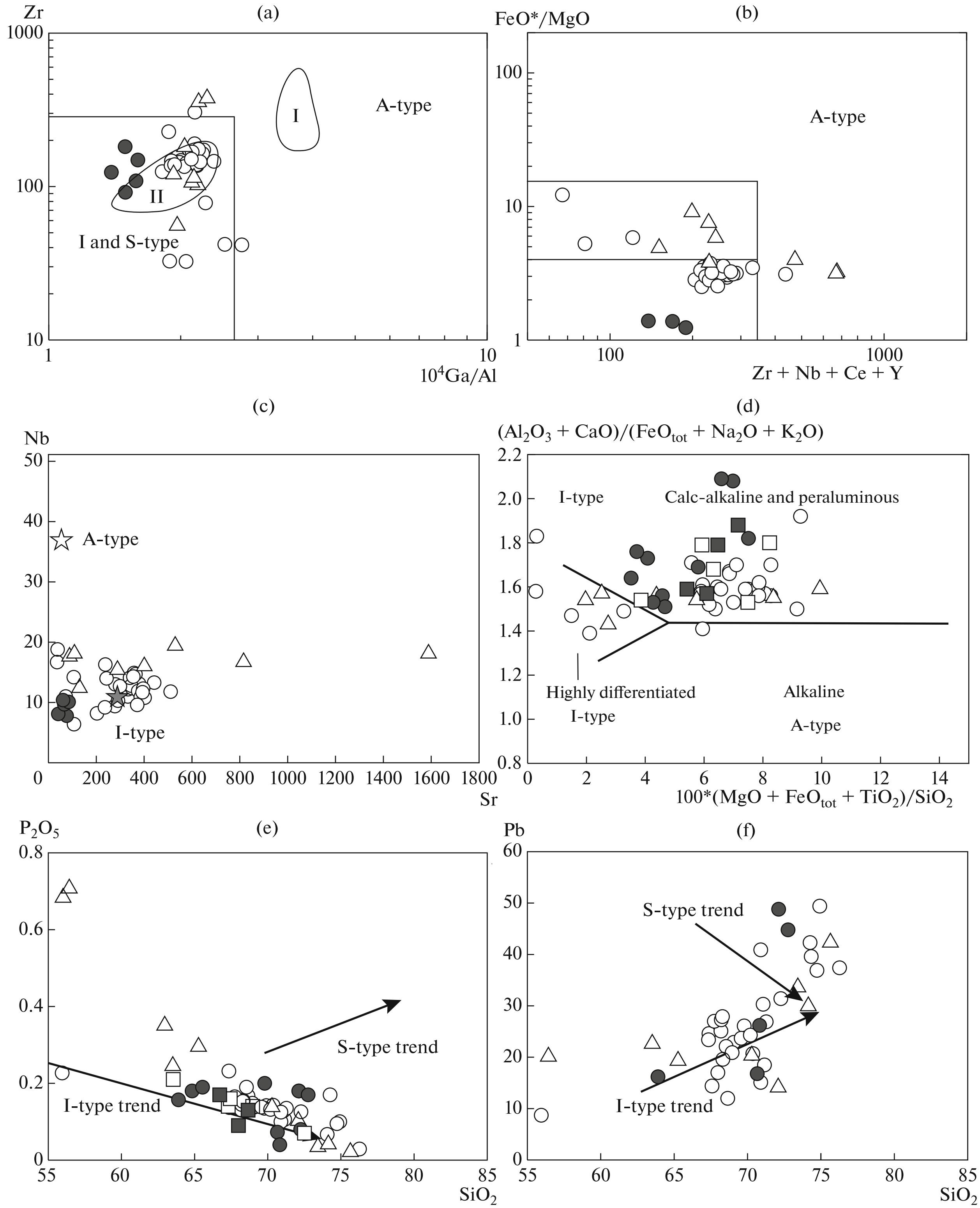

Fig. 7. Diagrams Zr–10^4Ga/Al (a), FeO_{tot}/MgO – Zr + Nb + Ce + Y (b) (Whalen et al., 1987), Nb–Sr (Whalen et al., 1987) (c), $(Al_2O_3 + CaO)/(FeO_{tot} + Na_2O + K_2O)$–100(MgO + FeO + TiO_2)/SiO_2 (Sylvester, 1989) (d), P_2O_5–SiO_2 (e), and Pb–SiO_2 (Chappell and White, 1992) (f) for the granitoids of the Kibera and Kuekvun massifs, granite pebble from conglomerate at the base of the Lower Carboniferous rocks. Fields of highly differentiated granites of I-type and A-type alkaline granites in (a) after (Chen et al., 2013); fields in (d) after (Sylvester, 1989); trends in (e, f) after (Chappell and White, 1992). Symbols are shown in Fig. 2.

sponding to trondhjemites, tonalites, and less siliceous rocks. The K_2O contents are below 1.0 wt %. Low-pressure ($P < 10$ kbar) melting of metabasites generates low-Al tonalites and trondhjemites (Arth, 1979), whereas high-Al varieties are formed at higher pressures. Anatectic melts obtained by melting of quartz amphibolite have higher SiO_2 contents, approximately equal Na and K contents, and moderate aluminum content.

Experiments on the dehydration melting of tonalitic rocks performed by Singh and Johannes (1996 a, b) are discussed in (Kruk, 2015). It is noted that the anatectic melts have 68–70% SiO_2, elevated CaO contents, moderate Al_2O_3, and weak K predominance over Na. Above mentioned authors (Clemens et al., 2011; Chappell et al., 2012) believe that magmas producing moderately peraluminous I-type granites are formed through partial melting of biotite–amphibole-bearing protolith (intermediate volcanic rocks) and during their ascent entrap peritectic products of melting reaction (clinopyroxene, plagioclase, ilmenite/Ti-magnetite), as well as residual zircon and apatite. High-K granitic magmas of I-type are formed by partial melting of high-K andesite–dacite (tonalite) rocks (Roberts and Clemens, 1993). In addition, the genesis of I-type calc-alkaline granite magmas is usually explained by crustal assimilation of mantle mafic magmas, fractionation of mantle magmas, or mixing of crustal and mantle magmas (Clemens et al., 2011).

The qualitative comparison of petrochemical characteristics of granitoids of the considered massifs with presented above experimental melting products of metabasites shows their difference and suggests their derivation from a different protolith. Application of major-element diagrams shows that most part of data points of the granitoids of the Kibera Massif and granite pebble fall in the field of melts obtained by partial melting of metagraywackes (Fig. 13a) or tonalites, partially, quartz amphibolites (Fig. 13b). The most siliceous compositions plot in the field of melting products of metapelites in both diagrams (Fig. 13). Data points of the granitoids of the Kuekvun Massif show a wider scatter in the diagrams in Fig. 13, falling in the regions of anatectic melts from amphibolites, metagraywackes, and metapelites. For comparison, we plotted the composition field of the Aptian–Albian granitoids of the Alyarmaut Uplift of Chukotka, which also have heterogeneous but more mafic composition of protolith (Fig. 13).

Our Sr–Nd–Pb isotope data on the granitoids in combination with the Hf isotope composition of zircons indicate contribution of both mantle and crustal material in parental granitoid melts. This also follows from insignificant negative εNd(T) values, which are intermediate between I- and S-type granites, values of initial $^{87}Sr/^{86}Sr$ ratio, wide variations of Pb isotope ratios, εHf in zircons from granites, and linear covariations of $^{207}Pb/^{204}Pb$ and $^{206}Pb/^{204}Pb$ (Figs. 10, 11).

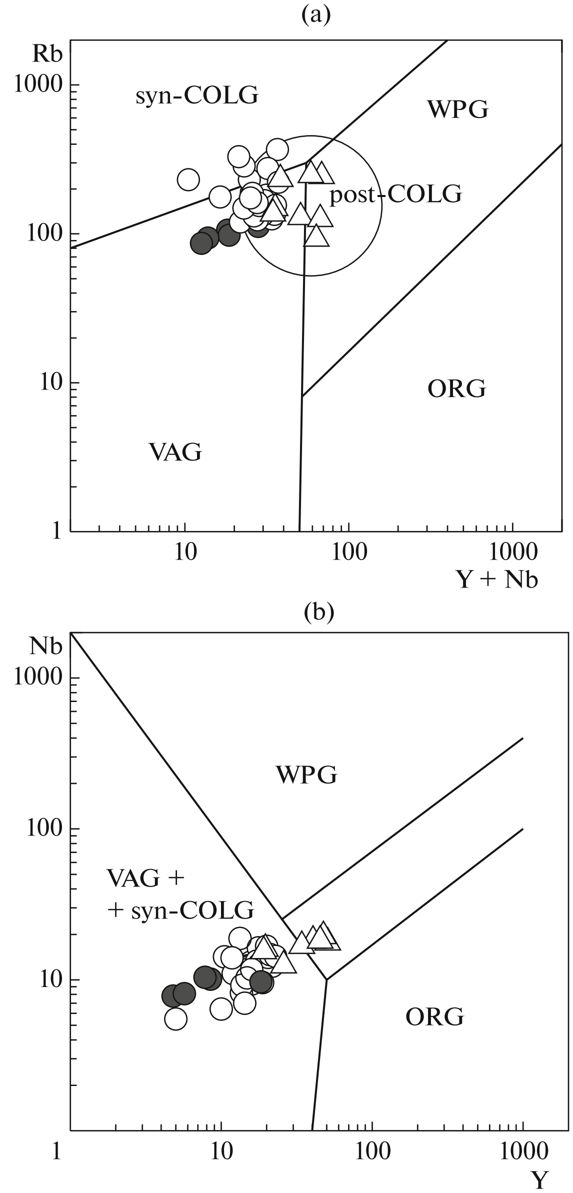

Fig. 8. Diagrams Rb–(Y + Nb) (a) and Y–Nb (b) (Pearce et al., 1984) for the granitoids of the Kibera and Kuekvun massifs, granite pebble from conglomerate at the base of the Lower Carboniferous rocks. Granites: (VAG) volcanic arc granites, (syn-COLG) syn-collisional granites, (WPG) within-plate granites, (ORG) oceanic ridge granites. Symbols are shown in Fig. 2.

The values of single- and two-stage Nd and Hf model ages of the granitoids suggest Meso–Paleoproterozoic age of crustal protolith, as do the Pb-Pb isochron model (1133 ± 470 Ma). Granitoids of the Alyarmaut Uplift have similar single-stage Nd model age (Luchitskaya et al., 2010). In addition, as recently established by (Luchitskaya et al., 2016), inherited Mesoproterozoic zircons are also present in the Neoproterozoic granitoids of the metamorphic basement of Wrangel Island.

Table 2. Sr–Nd–Pb isotope composition of granitoids from the Kibera and Kuekvun massifs and granite pebble from conglomerate at the base of the Lower Carboniferous rocks

Sample	Rb, ppm	Sr, ppm	$^{87}Rb/^{86}Sr$	$^{87}Sr/^{86}Sr$	± 2S	Sm, ppm	Nd, ppm	$^{147}Sm/^{144}Nd$	$^{143}Nd/^{144}Nd$	± 2S	$^{87}Sr/^{86}Sr$*	$^{143}Nd/^{144}Nd$*
K-10-8	169	405	1.20900	0.712974	0.000004	4.44	25.5	0.10524	0.512351	0.000002	0.706899	0.512107
K-10-61	155	388	1.15892	0.713095	0.000005	4.57	25.8	0.10705	0.512348	0.000002	0.707271	0.512100
K-10-72	159	303	1.52096	0.714771	0.000003	3.63	20.2	0.10848	0.512374	0.000002	0.707128	0.512123
K-10-80	145	380	1.10241	0.713385	0.000007	4.85	28.2	0.10397	0.512352	0.000003	0.707845	0.512111
K-10-92	259	437	1.71547	0.714509	0.000010	3.04	17.1	0.10728	0.512382	0.000002	0.705889	0.512134
K-10-189	148	932	0.45849	0.709325	0.000004	13.6	85.7	0.09610	0.512353	0.000002	0.707021	0.512131
K-10-194	130	641	0.58718	0.710189	0.000003	17.1	108	0.09605	0.512353	0.000002	0.707239	0.512131
K-10-217	172	590	0.84337	0.710689	0.000004	4.96	30.4	0.09852	0.512355	0.000003	0.706451	0.512127
K-10-83	277	62.9	12.8113	0.771753	0.000009	1.34	4.95	0.16318	0.512414	0.000003	0.707374	0.512037
K-10-29/7	119	58.9	5.86000	0.724492	0.000007	4.04	25.7	0.09522	0.512294	0.000002	0.695045	0.512074

Sample	$\varepsilon_{Nd}(T)$	TDM1	TDM2	$^{206}Pb/^{204}Pb$	± 2S	$^{207}Pb/^{204}Pb$	± 2S	$^{208}Pb/^{204}Pb$	± 2S	$^{206}Pb/^{204}Pb$*	$^{207}Pb/^{204}Pb$*	$^{208}Pb/^{204}Pb$*
K-10-8	–1.49	1125	1247	19.5627	0.0002	15.6615	0.0002	39.3947	0.0005	nd	nd	nd
K-10-61	–1.62	1148	1258	18.7271	0.0002	15.6016	0.0002	39.0878	0.0005	18.5193	15.5905	38.1467
K-10-72	–1.17	1126	1221	18.8615	0.0002	15.6022	0.0001	38.9681	0.0004	nd	nd	nd
K-10-80	–1.41	1111	1240	18.7333	0.0005	15.6030	0.0006	38.9079	0.0022	18.4615	15.5884	37.9450
K-10-92	–0.95	1101	1203	19.2158	0.0005	15.6418	0.0006	39.3570	0.0020	19.8012	15.6958	38.3431
K-10-189	–1.02	1035	1208	19.0710	0.0002	15.6105	0.0002	40.1312	0.0005	16.9871	15.5224	36.4599
K-10-194	–1.02	1034	1208	19.1177	0.0002	15.6214	0.0002	40.5115	0.0008	18.4510	15.5773	37.9092
K-10-217	–1.09	1054	1214	19.4393	0.0002	15.6425	0.0002	39.5055	0.0005	18.6373	15.5957	37.7765
K-10-83	–2.86	2218	1361	20.1301	0.0003	15.7134	0.0002	38.4355	0.0008	18.8598	15.6115	38.0703
K-10-29/7	–2.13	1102	1300	18.6909	0.0004	15.6157	0.0004	38.7637	0.0009	18.5063	15.6058	38.1428

$^{87}Sr/^{86}Sr$*, $^{143}Nd/^{144}Nd$*, $^{206}Pb/^{204}Pb$*, $^{207}Pb/^{204}Pb$*, $^{208}Pb/^{204}Pb$* correspond to values of isotope composition at 353 Ma. Value of $\varepsilon_{Nd}(T)$ was calculated relative to chondrite uniform reservoir (CHUR): $^{147}Sm/^{144}Nd = 0.1967$ and $^{143}Nd/^{144}Nd = 0.512638$, $^{87}Rb/^{86}Sr = 0.08160$, $^{87}Sr/^{86}Sr = 0.70450$. Model ages T_{DM1} and T_{DM2} were calculated using following characteristics of the depleted mantle reservoir (DM): $^{147}Sm/^{144}Nd = 0.2136$ and $^{143}Nd/^{144}Nd = 0.513151$; $^{147}Sm/^{144}Nd = 0.12$ was taken for continental crust.

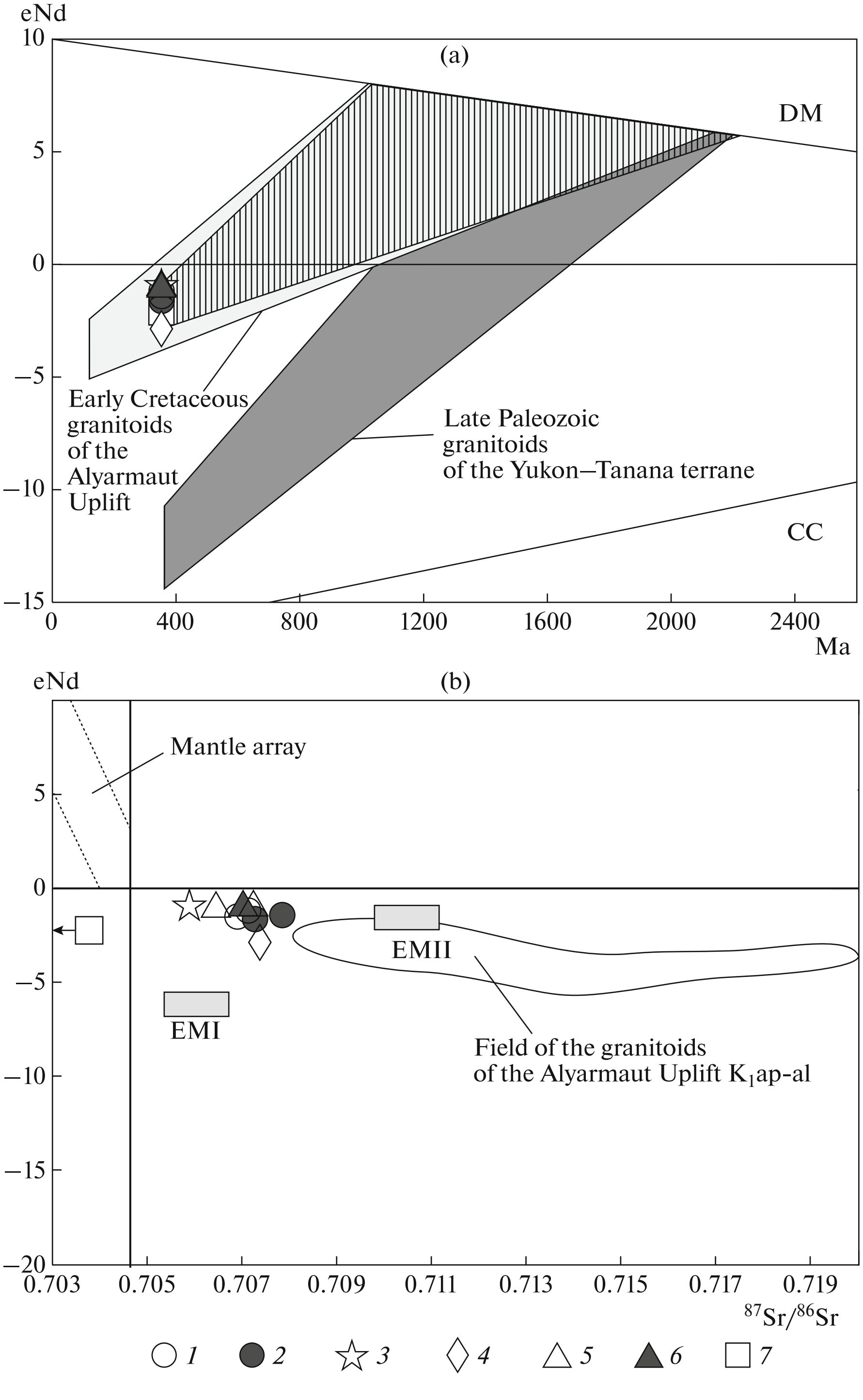

Fig. 9. Diagram εNd(T)–time (a) and εNd(T)–$^{87}Sr/^{86}Sr$ (b) for the granitoids of the Kibera and Kuekvun massifs and granite pebble from conglomerate at the base of the Lower Carboniferous rocks. (DM) depleted mantle; (CC) continental crust; (EMI, EMII) end mantle components: (EMI) enriched mantle with high Rb/Sr, (EMII) enriched mantle with high Nd/Sm. (*1–4*) granitoids of the Kibera Massif: (*1*) granite, (*2*) granodiorite, (*3*) monzonite from enclaves, (*4*) alaskite; (*5*, *6*) granitoids of the Kuekvun Massif: (*5*) granodiorite, (*6*) quartz monzodiorite; (*7*) granite pebble.

Granitoid melts formed by partial melting of heterogeneous source were subjected to fractional crystallization, which was accompanied by a decrease of TiO_2, MgO, CaO, FeO_{tot}, Al_2O_3 contents, growth of Rb contents, and decrease of Sr content (Fig. 4a), which led to the formation of highly-differentiated I-type granites. Covariations of Ba and Sr, TiO_2 and Zr, (La/Yb)n–La suggest the fractionation of pla-

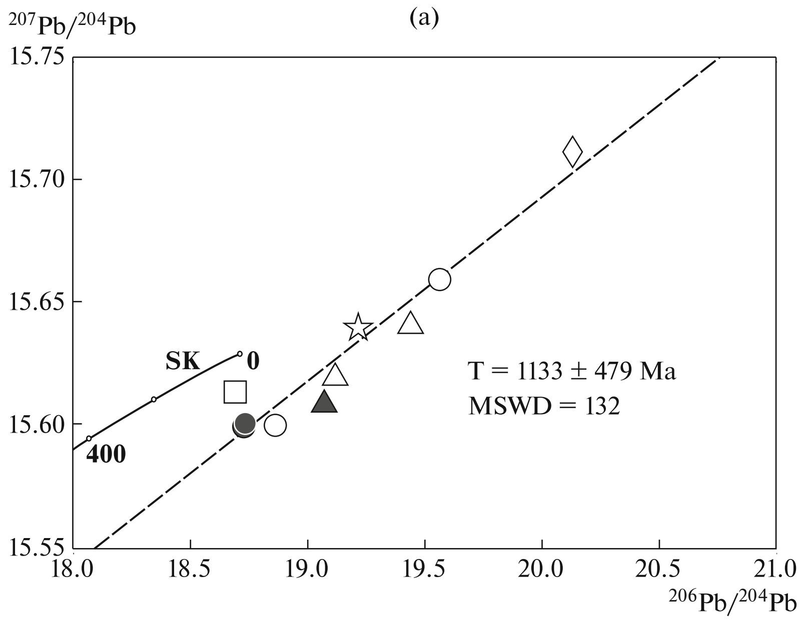

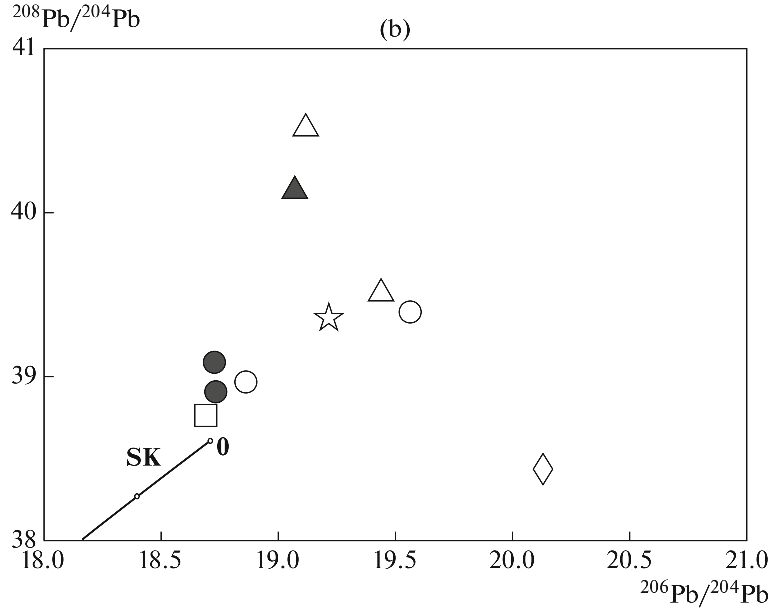

Fig. 10. Diagram $^{207}Pb/^{204}Pb-^{206}Pb/^{204}Pb$ (a) and $^{208}Pb/^{204}Pb-^{206}Pb/^{204}Pb$ (b) for the granitoids of the Kibera and Kuekvun massifs, granite pebble from conglomerate at the base of the Lower Carboniferous rocks. (SK) two-stage evolution curve for crustal lead using model (Stacey and Kramers, 1975). Symbols are shown in Fig. 9.

gioclase, hornblende, biotite, K-feldspar, and accessory magnetite, titanite, and allanite (Fig. 4b). This is confirmed by the negative Ba, Sr, and Ti anomalies in the spidergrams of granitoids of both the massifs and correspondence of data points to the trend of I-type granites in the $P_2O_5-SiO_2$ and $Pb-SiO_2$ diagrams (Figs. 7e, 7f). Negative P anomaly in the spidergrams points to the apatite separation (Fig. 6).

The high-K alkali-calcic and calc-alkaline granitoids of I-type, including their highly evolved varieties, are likely formed in an Andean-type continental margin setting (Ruks et al., 2006; Cheong et al., 2002; Shaw et al., 2014, etc.).

According to the tectonic reconstructions proposed for the Anyui–Chukotka fold system, as for the entire Arctic region, Chukotka and Arctic Alaska represented a single block or microcontinent, which collided with the North Asian margin owing to the closure of the South Anyui Ocean in the Early Cretaceous (Zonenshain et al., 1991; Natal'in et al., 1999; Sokolov et al., 2015). The movement of this block began with the opening of the Canadian basin in the Late Jurassic, and its rotation is regarded as the generally

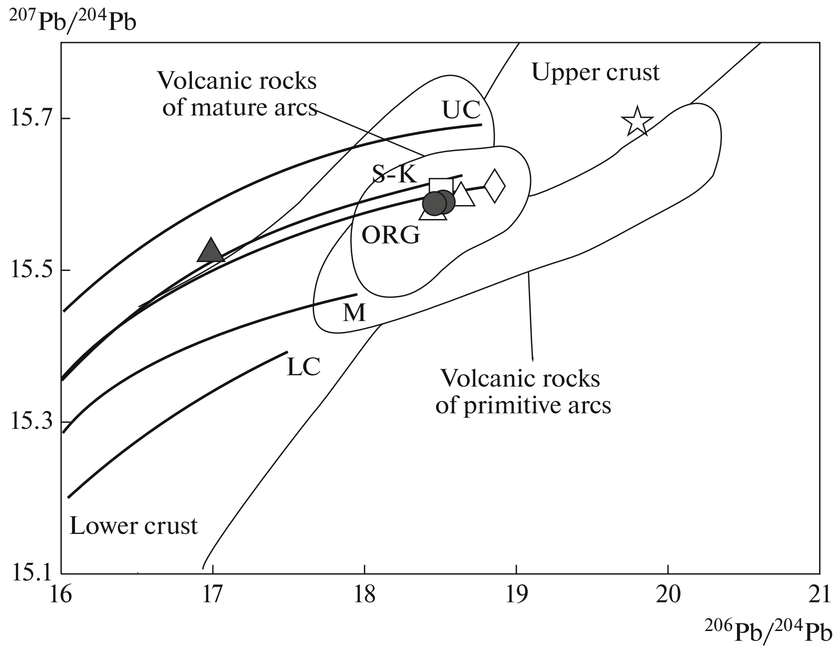

Fig. 11. Diagram $^{207}Pb/^{204}Pb$–$^{206}Pb/^{204}Pb$ for granitoids of the Kibera and Kuekvun massifs, and granite pebble from conglomerate at the base of the Lower Carboniferous rocks. Shown lines demonstrate Pb evolution in different reservoirs: (LC) lower crustal, (M) mantle, (ORG) orogenic, (UC) upper crustal, (S-K) evolution curve of terrestrial lead after two-stage model (Stacey and Kramers, 1975). Fields of model sources: lower and upper crustal, mature, and primitive island arcs. Symbols are shown in Fig. 9.

accepted mechanism of its movement (Grantz et al., 1991, 2011; Lawver et al., 2002).

The Devonian–Early Carboniferous granitoids of similar age are traced in different regions of the Chukotka–Arctic Alaska block: Koolen dome in East Chukotka (369–375 Ma, Natal'in et al., 1999), Seward Peninsula in Alaska (403–378 Ma), and Brooks Range of Arctic Alaska (400–370 Ma) (Luchitskaya et al., 2015). According to (Natal'in et al., 1999), the Late Devonian granitoids of the Koolen Dome belonged to the magmatic arc located on the southern margin of the Precambrian Bennet–Barrovian or Arctida block (basement of the Chukotka–Arctic Alaska microcontinent) after its collision with the margin of the North American Craton in the Early Devonian, which led to the Ellesmere orogenesis of the North Alaska and Canadian Arctic Islands. According to (Natal'in et al., 1999), this magmatic arc, in addition to the plutonic rocks, contains differentiated calc-alkaline volcanic rocks (andesites and their tuffs).

Thus, obtained petrogeochemical data on the Early Carboniferous granitoids of the Kibera and Kuekvun massifs and their affiliation to the I-type granites are consistent with the existence of the Late Devonian–Early Carboniferous marginal-continental magmatic arc on the southern Arctida margin. The Sr–Nd–Pb–Hf isotope composition of the granitoids indicates the contribution of both mantle and crustal component in the formation of their source and points to the marginal–continental setting of granitoid magmatism formed by interaction of melts derived from suprasubduction mantle wedge with continental crust. In particular, the range of zircon εHf (from –5.3 to +12.1) and initial $^{87}Sr/^{86}Sr$ (0.70322–0.70728) in the Jurassic–Cretaceous Peninsula Range and Sierra Nevada batholiths of the North American continental margin (Lee et al., 2007; Shaw et al., 2014) are comparable to those of the Kibera and Kuekvun granite massifs (from –5.2 to +16.7 and 0.70588–0.70784, respectively). It is suggested that $^{87}Sr/^{86}Sr$ = 0.706 in granitoids is boundary value separating the blocks with ancient continental and accretionary–island arc (juvenile) crusts. As compared to the Late Paleozoic granitoids from the same margin, a source of the granitoids of the Kibera and Kuekvun massifs demonstrate a lesser contribution of ancient crustal material.

CONCLUSIONS

(1) Petrographic, petrogeochemical, and isotope compositions of the granitoids of the Kibera and Kuekvun massifs and granite pebble from conglomerates at the base of the Lower Carboniferous sequence indicate their affiliation to I-type granites (Chappell and White, 1992), including their highly evolved varieties.

Table 3. Lu-Hf isotope composition of zircons in the granitoids of the Kiber, Kuekvun massifs and pebble at the base of the Lower Carboniferous sediments.

Sample and point no.	T, Ma	$^{176}Lu/^{177}Hf$	$^{176}Yb/^{177}Hf$	$^{176}Hf/^{177}Hf$	Hfi	Epsilon	Lse	T(DM)	T(DM)C
k-10-27-06	360	0.003178	0.129412	0.283439	0.283418	30.4	1.4	–0.29	–0.55
k-10-27-09	360	0.001497	0.033328	0.282754	0.282744	6.5	0.7	0.72	0.88
k-10-27-10	360	0.002193	0.075476	0.283045	0.283030	16.7	2.6	0.30	0.28
k-10-27-13	360	0.001474	0.047283	0.282944	0.282934	13.3	0.7	0.44	0.48
k-10-27-18	360	0.001148	0.031863	0.282776	0.282768	7.4	0.5	0.68	0.83
k-10–27-22	360	0.001543	0.062422	0.283025	0.283015	16.1	1.4	0.33	0.31
k-10-9-09	352	0.003178	0.129412	0.283439	0.283418	30.2	1.4	-0.29	-0.54
K-10-9-09	352	0.001174	0.043735	0.282734	0.282726	5.8	0.6	0.74	0.92
K-10-9-14	352	0.000975	0.033957	0.282727	0.282721	5.6	0.4	0.74	0.93
K-10-9-16	352	0.001012	0.039457	0.282840	0.282833	9.5	0.7	0.58	0.70
K-10-9-18	352	0.001417	0.058007	0.283009	0.283000	15.4	0.9	0.35	0.35
K-10-9-21	352	0.001509	0.057396	0.283021	0.283011	15.8	0.6	0.33	0.32
K-10-9-22	352	0.001136	0.044585	0.282823	0.282816	8.9	1.4	0.61	0.74
K-10-9-24	352	0.001560	0.062158	0.282938	0.282928	12.9	1.5	0.45	0.50
K-10-9-29	352	0.001228	0.046430	0.282798	0.282790	8.0	0.7	0.65	0.79
K-10-9-30	352	0.000705	0.019872	0.282420	0.282415	–5.2	0.4	1.17	1.57
K-10-9-32	352	0.001450	0.048023	0.282528	0.282518	–1.6	0.4	1.04	1.36
K-10-9-33	352	0.001462	0.048406	0.282522	0.282512	–1.8	0.4	1.05	1.37
K-10-9-34	352	0.001617	0.049365	0.282569	0.282558	–0.2	0.4	0.98	1.27
K-10-9-36	352	0.001861	0.065127	0.282649	0.282637	2.6	0.5	0.87	1.11
K-10-73-04	357	0.001528	0.053922	0.282835	0.282825	9.4	0.5	0.60	0.71
K-10-73-06	357	0.002307	0.080853	0.282914	0.282899	12.0	0.7	0.50	0.56
K-10-73-09	357	0.002372	0.096860	0.283074	0.283058	17.6	1.5	0.26	0.22
K-10-73-10	357	0.001583	0.054760	0.282906	0.282895	11.9	0.5	0.50	0.57
K-10-73-14	357	0.001094	0.040129	0.282802	0.282795	8.3	0.4	0.64	0.78
K-10-73-23	357	0.001088	0.039709	0.282772	0.282765	7.2	0.5	0.68	0.84
K-10-73-24	357	0.002541	0.102926	0.283048	0.283031	16.7	0.7	0.30	0.28
K-10-73-27	357	0.001491	0.053167	0.282799	0.282789	8.1	0.5	0.65	0.79
K-10-73-29	357	0.001088	0.036472	0.282769	0.282762	7.1	0.4	0.69	0.85
K-10-73-31	357	0.001132	0.041208	0.282774	0.282766	7.3	0.6	0.68	0.84
K-10-73-31	357	0.001884	0.049228	0.282803	0.282790	8.1	0.6	0.65	0.79
K-10-73-33	357	0.000915	0.032571	0.282689	0.282683	4.3	0.5	0.80	1.01
K-10-73-42	357	0.001497	0.055326	0.282797	0.282787	8.0	0.8	0.65	0.79
K-10-73-49	357	0.001417	0.051336	0.282793	0.282784	7.9	0.6	0.66	0.80

$^{176}Lu/^{177}Hf$ CHUR =0.0336 ± 1, $^{176}Hf/^{177}Hf$ CHUR = 0.282785 ± 11 (Bouvier et al., 2008). Decay constant of 176Lu after (Sherer et al., 2001).

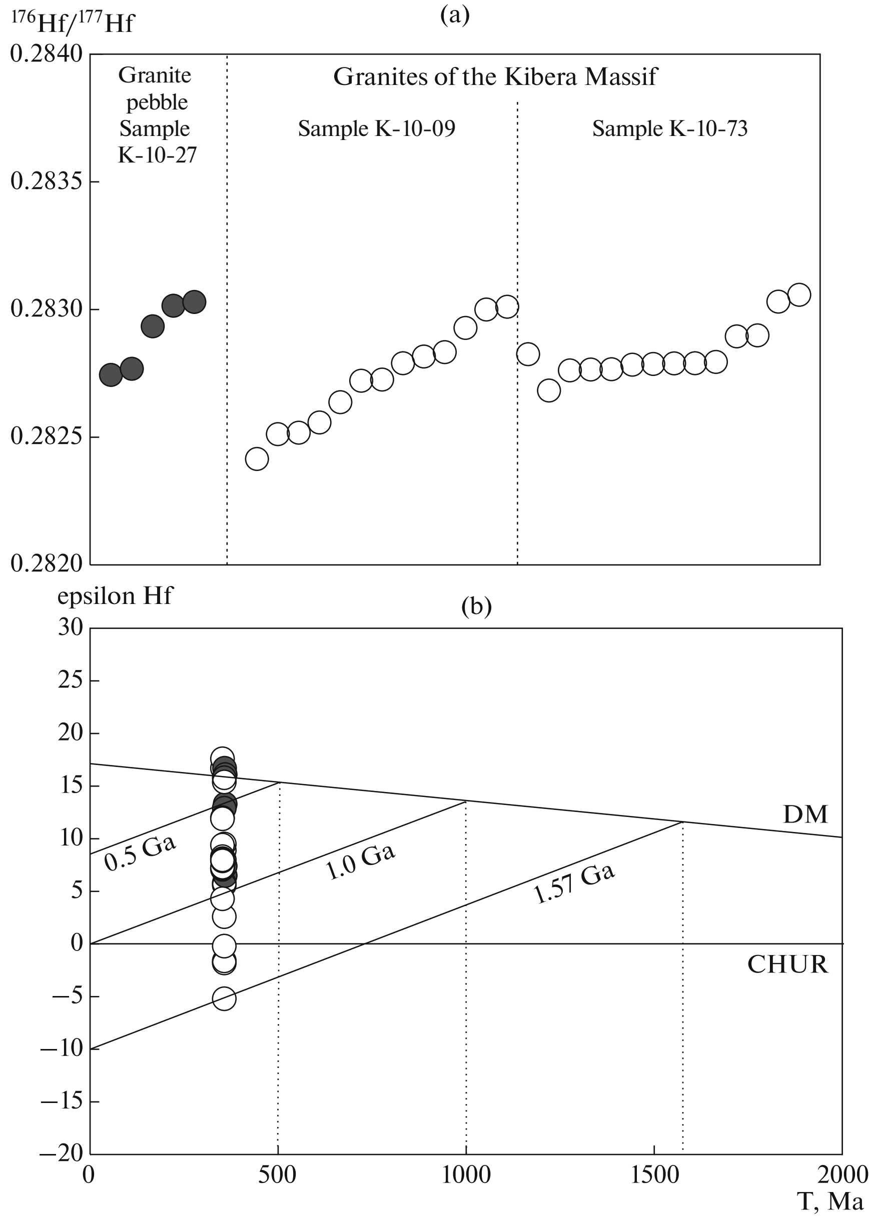

Fig. 12. Diagram $^{176}Hf/^{177}Hf$–time (a) and εHf–time (b) for granites of the Kibera Massif (sample K-10-9, K-10-73) and granite pebble at the base of the Lower Carboniferous rocks.

(2) Sr–Nd–Pb isotope composition of the granitoids of both the massifs and granite pebble and Hf isotope composition of zircons indicate the contribution of both mantle and crustal component in the formation of source of parental granitoid melts.

(3) The comparison of compositions of the granitoids with compositions of melts formed by partial melting of diverse protoliths also reveals a heterogeneous character of protolith, which could include both metagraywacke or tonalite, and amphibolite or quartz amphibolite, partially metapelite.

(4) Granitoid melts formed by partial melting of a heterogeneous source experienced fractional crystallization with decreasing TiO_2, MgO, CaO, FeO_{tot}, Al_2O_3, Sr, growth of Rb, fractionation of plagioclase, hornblende, biotite, K-feldspar, and accessory magnetite, titanite, allanite, apatite, and formation of highly differentiated I-type granites.

(5) The granitoids of the Kibera and Kuekvun massifs were likely formed in the Andean-type continental margin setting, which is consistent with the inferred existence of the Late Devonian–Early Carboniferous marginal continental magmatic arc on the southern margin of Arctida, which is reconstructed on the basis of the presence of differentiated calc-alkaline volcanic rocks of the corresponding age

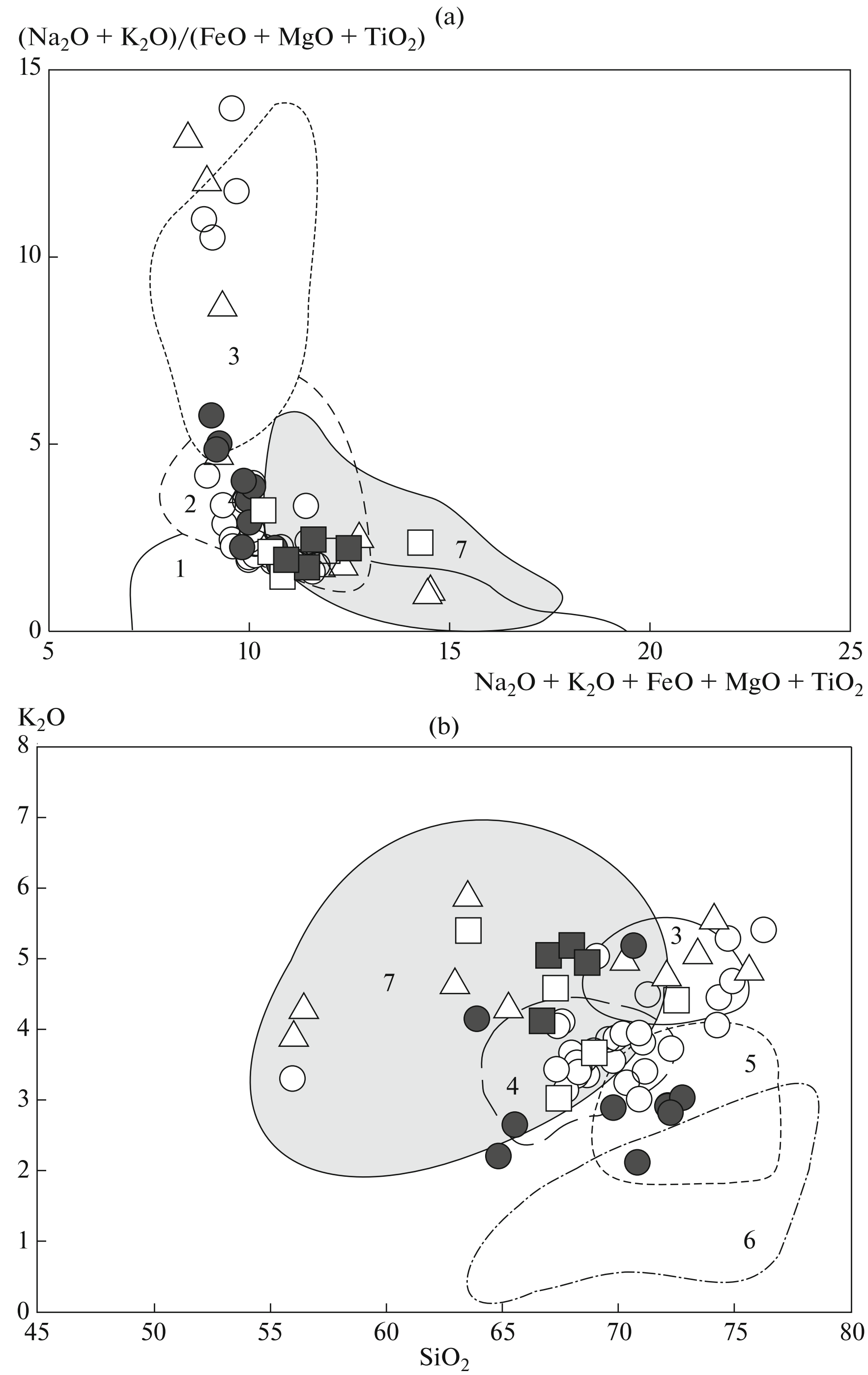

Fig. 13. Diagrams $(Na_2O + K_2O)/(FeO + MgO + TiO_2)$ – $Na_2O + K_2O + FeO + MgO + TiO_2$ (a) and K_2O–SiO_2 (b) for granitoids of the Kibera and Kuekvun massifs and granite pebble from conglomerate at the base of the Lower Carboniferous rocks. (1–4) composition fields of anatectic melts derived by partial melting: (1) amphibolite, (2) metagraywacke, (3) metapelite, (4) metatonalite, (5) quartz amphibolite, (6) metabasite; (7) composition field of the granitoids of the Alyarmaut Uplift. Symbols are shown in Fig. 2.

(Natal'in et al., 1999). Isotope data on the granitoids also support the marginal–continental setting of granitoid magmatism, when melt formed by melting of suprasubduction mantle wedge interacted with continental crust.

ACKNOWLEDGMENTS

We are grateful to S.A. Silantyev and anonymous reviewer for attention to our paper and useful recommendations.

This work was supported by the Russian Foundation for Basic Research (project nos. 13-05-00249, 16-05-00146), Leading Scientific School (NSh-9581.2016.5) and State Task on Theme "Origin and tectonic evolution of Arctic and Pacific structures of the Northeast Russia".

REFERENCES

V. V. Akinin, "New geochronological data on pre-Mesozoic rocks (Neoproterozoic to Devonian) of Arctic Chukotka," *ICAM-VI Abstracts*, 95 (2011).

J. G. Arth, "Some trace elements in trondhjemites: their implications to magma genesis and paleotectonic settings," in *Trondhjemites, Dacites, and Related Rocks,* Ed. by F. Barker (Elsevier, Amsterdam, 1979), pp. 123–132.

A. Bouvier, J. D. Vervoort, and J. Patchett, "The Lu-Hf and Sm-Nd isotopic composition of CHUR: constraints from unequilibrated chondrites and implications for the bulk composition of terrestrial planets," Earth Planet. Sci. Lett. **273**, 48–57(2008).

B. W. Chappell and A. J. R. White, "I- and S-type granites in the Lachlan Fold Belt," Trans. R. Soc. Edinb.: Earth Sci. **83**, 1–26 (1992).

B. W. Chappell, C. J. Bryant and D. Wyborn, "Peraluminous I-type granites," Lithos **158**, 142–153 (2012).

J.-Y. Chen, J.-H. Yang, J.-H. Zhang, J.-F. Sun, and S. A. Wilde, "Petrogenesis of the Cretaceous Zhangzhou batholith in southeastern China: zircon U-Pb age and Sr-Nd-Hf-O isotopic evidence," Lithos **162–163**, 140–156 (2013).

C.-S. Cheong, S.-T. Kwon, and H. Sagong, "Geochemical and Sr-Nd-Pb isotopic investigation of Triassic granitoids and basement rocks in the northern Gyeongsang Basin, Korea: implications for the young basement in the East Asian continental margin," The Island Arc, No. **11**, 25–44 (2002).

J. D. Clemens, G. Stevens, and F. Farina, "The enigmatic sources of I-type granites: the peritectic connexion," Lithos **126**, 174–181 (2011).

A. Cocherie, "Systematic use of trace element distribution patterns in log–log diagrams for plutonic suites," Geochim. Cosmochim. Acta **50**, 2517–2522 (1986).

V. G. Ditmar, "Geological structure of the northern Chukchi region," Tr. Arktich. Inst. **95**, 5–85 (1938).

B. R. Frost, C. G. Barnes, W. J. Collins, R. J. Arculus, D. J. Ellis, and C. D. Frost, "A geochemical classification for granitic rocks," J. Petrol. **42** (11), 2033–2048 (2001).

M. L. Gelman, "Phanerozoic granite-metamorphic cupolas in northeastern Siberia. Paper 1. Geological history of Paleozoic and Mesozoic cupolas," Tikhookean. Geol. **14** (4), 102–115 (1995).

Geodynamics, Magmatism, and Metallogeny of East Russia, Ed. by A. I. Khanchuk (Dal'nauka, Vladivostok, 2006), **Vol. 1**, pp. 1–572 [in Russian].

A. Grantz, P. E. Hart, and V. A. Childers, "Geology and tectonic development of the Amerasia and Canada basins, Arctic Ocean," in *Arctic Petroleum Geology,* Ed. by A. M. Spencer, A. F. Embry, D. L. Gautier, A. V. Stoupakova, and K. Sorensen, Geol. Soc. London Mem. **35**, 771–800 (2011).

A. Grantz, T. E. Moore, and S. M. Roeske, *Gulf of Alaska to Arctic Ocean: Geological Society of America Continental-Ocean Transect A-3, Scale 1 : 500000* (Menlo Park, 1991).

S. M. Katkov, M. V. Luchitskaya, A. B. Kotov, E. B. Sal'nikova, and S. Z. Yakovleva "Late Paleozoic granitoids of Central Chukotka: structural position and age constraints," Dokl. Earth Sci. **450** (1), 484–488 (2013).

N. N. Kruk, Extended Abstract of Doctoral Dissertation in Geology and Mineralogy (IGM SO RAN, Novosibirsk, 2015) [in Russian].

N. A. Kulyukina, P. L. Tikhomirova, and V. O. Yapaskurt, "New data on the metamorphic petrology of rocks from the Kuekvun Uplift (northern Chukchi Peninsula)," Mosc. Univ. Geol. Bull. **68** (2), 89–95 (2013).

N. B. Kuznetsov, L. M. Natapov, E. A. Belousova, W. L. Griffin, and S. Y. O'Reilly, "First isotopic data on detrital zircons from the Engane-Pe Uplift (western Polar Urals): implications for the primary tectonic position of the Pre-Uralides–Timanides," Dokl. Earth Sci. **426** (4), 567–573 (2009).

L. S. Lane, M. P. Cecile, G. E. Gehrels, M. K. Kos'ko, P. W. Layer, and R. R. Parrish, "Geochronology and structural setting of latest Devonian–Early Carboniferous magmatic rocks, Cape Kiber, northeast Russia," Can. J. Earth Sci. **52**, 147–160 (2015).

L. A. Lawver, A. Grantz, and L. M. Gahagan, "Plate kinematic evolution of the present Arctic Region since the Ordovician," in *Tectonic evolution of the Bering Shelf-Chukchi Sea-Arctic Margin and Adjacent Landmasses,* Ed. by E. L. Miller, S. Klemperer, and A. Grantz, Geol. Soc. Am., 2002), pp. 333–358.

S. Li, T. Wang, S. A. Wilde, Y. Tong, D. Hong, and Q. Guo, "Geochronology, petrogenesis and tectonic implications of Triassic granitoids from Beishan, NW China," Lithos **134–135**, 123–145 (2012).

M. V. Luchitskaya, S. D. Sokolov, A. B. Kotov, L. M. Natapov, E. A. Belousova, and S. M. Katkov, "Late Paleozoic granitic rocks of the Chukchi Peninsula: composition and location in the structure of the Russian Arctic," Geotectonics **49** (4), 243–268 (2015).

M. V. Luchitskaya, S. D. Sokolov, G. E. Bondarenko, and S. M. Katkov, "Composition and geodynamic setting of granitoid magmatism in the Alyarmaut Uplift, western Chukchi Peninsula," Geochem. Int. **48** (9), 891–916 (2010).

E. A. K. Middlemost, "Naming materials in magma/igneous rock system," Earth Sci. Rev. **37**, 215–224 (1994).

B. A. Natal'in, J. M. Amato, J. Toro, and J. E. Wright, "Paleozoic rocks of northern Chukotka Peninsula, Russian Far East: implications for the tectonic of Arctic region," Tectonics **18** (4), 977–1003 (1999).

J. A. Pearce, "Sources and settings of granitic rocks," Episodes **19** (4), 120–125 (1996).

J. A. Pearce, N. B. W. Harris, and A. G. Tindle, "Trace element discrimination diagrams for the tectonic interpretation of granitic rocks," J. Petrol. **25** (4), 956–983 (1984).

A. Peccerillo and S. R. Taylor, "Geochemistry of Eocene calc-alkaline volcanic rocks from the Kastamonu area, northern Turkey," Contrib. Mineral. Petrol. **58**, 63–81 (1976).

C. Pin, S. Joannon, C. Bosq, B. Le Fevre, and P. Gauthier, "Precise determination of Rb, Sr, Ba, and Pb in geological materials by isotope dilution and ICP-quadrupole mass spectrometry following selective separation of the analytes," J. Anal. At. Spectrom. **18**, 135–141 (2003).

G. O. Polzunenkov, V. V. Akinin, and I. Yu. Cherepanova, "New data on the age and composition of the Velitkenai and Kuekvun granite gneiss massifs (Arctic Chukchi): application to the development of model of granitoid mineralization," in *Gold of the Northern Pacific Framing. Proceedings of 2nd International Mining-Geological Forum Devoted to the 100th Yu.A. Bilibin, Magadan, Russia, 2011* (SVKNII DVO RAN, 2011), pp. 170–171 [in Russian].

P. Richard, N. Schimizu, and C. J. Allegre, "$^{143}Nd/^{146}Nd$ a natural tracer: an application to oceanic basalts," Earth Planet. Sci. Lett. **31** (2), 269–278 (1976).

M. P. Roberts and J. D. Clemens, "Origin of high-potassium, calc-alkaline, I-type granitoids," Geology **21**, 825–828 (1993).

T. W. Ruks, S. J. Piercey, J. J. Ryan, M. E. Villeneuve, and R. A. Creaser, "Mid- to late Paleozoic K-feldspar augen granitoids of the Yukon-Tanana terrane, Yukon, Canada: implications for crustal growth and tectonic evolution of the northern Cordillera," GSA Bull. **118** (9–10), 1212–1231 (2006).

S. E. Shaw, V. R. Todd, D. L. Kimbrough, and N. J. Pearson, "A west-to-east geologic transect across the Peninsular Ranges batholith, San Diego County, California: zircon $^{176}Hf/^{177}Hf$ evidence for the mixing of crustal- and mantle-derived magmas, and comparisons with the Sierra Nevada batholiths," in *Peninsular Ranges Batholith, Baja California and Southern California,* Ed. by D. M. Morton and F. K. Miller, Geol. Soc. Amer. Mem. **211**, 499–536 (2014).

E. Sherer, C. Munker, and K. Mezger, "Calibration of the lutetium–hafnium clock," Science **27** (5530), 683–687 (2001).

J. Singh, "Dehydration melting of tonalities. Part I. Beginning of melting," Contrib. Mineral., Petrol. **125**, 16–25 (1996a).

J. Singh, "Dehydration melting of tonalities. Part II. Beginning of melting," Contrib. Mineral. Petrol. **125**, 25–44 (1996b).

S. D. Sokolov, M. I. Tuchkova, A. V. Ganelin, G. E. Bondarenko, and P. Layer, "Tectonics of the South Anyui suture, Northeastern Asia," Geotectonics, **49** (1), 3–26 (2015).

J. S. Stacey and J. D. Kramers, "Approximation of terrestrial lead isotope evolution by a two-stage model," Earth Planet. Sci. Lett. **26** (2), 207–221 (1975).

State Geological Map on a Scale 1 : 200 000. Anyui–Chaun Series. Sheets R-59-XXIII, XXIV. Explanatory Notes, Ed. by N. M. Samorukov and V. T. Matveenko, (Mingeo, Moscow, 1984) [in Russian].

S. S. Sun and W. F. McDonough, "Chemical and isotopic systematics of oceanic basalts: implications for mantle composition and processes," Geol. Soc. London. Spec. Publ. **42**, 313–345 (1989).

P. J. Sylvester, "Post-collisional alkaline granites," J. Geol. **97**, 261–280 (1989).

I. V. Tibilov, and I. Yu. Cherepanova, *Geology of the Northern Chukotka: Modern State and Problems* (GEOS, Moscow, 2001) [in Russian].

I. V. Tibilov, A. L. Milov, and I. A. Davydov, "Manifestation of Pre-Mesozoic granitoid magmatism in Chukotka," Tikhookean Geol., No. 4, 95–98 (1986).

O. M. Turkina, "Modeling geochemical types of tonalite–trondhjemite melts and their natural equivalents," Geochem. Int. **38** (7), 640–651 (2000).

V. A. Varlamova, G. M. Malysheva, B. V. Vyatkin, et al., *Information Report on Uncompleted Works on Object "Creation of Digital Geological Map Set on a Scale 1 : 500000 of the Chukchi Autonomous Region* (FGUGP Georegion, Anadyr, 2004) [in Russian].

V. E. Verzhbitsky, S. D. Sokolov, and M. I. Tuchkova, "Present-day structure and stages of tectonic evolution of Wrangel Island, Russian Eastern Arctic Region," Geotectonics **49** (3), 165–192 (2015).

J. B. Whalen, K. L. Currie, and B. W. Chappell, "A-type granites: geochemical characteristics, discrimination and petrogenesis," Contrib. Mineral. Petrol. **95** (4), 407–419 (1987).

L. P. Zonenshain, M. I. Kuzmin, and L. M. Natapov, *Tectonics of Lithospheric Plates of the USSR Territory* (Nauka, Moscow, 1990), vol. 2 [in Russian].

Translated by M. Bogina